100
(DOI: will be inserted by hand later)

Astronomy & Astrophysics

TOPoS: II. On the bimodality of carbon abundance in CEMP stars ⋆

Implications on the early chemical evolution of galaxies

P. Bonifacio[1], E. Caffau⋆⋆[1,2], M. Spite[2], M. Limongi[3,4], A. Chieffi[5], R.S. Klessen[6,7,8], P. François[1,9], P. Molaro[10], H.-G. Ludwig[2,1], S. Zaggia[11], F. Spite[1], B. Plez[12] R. Cayrel[1], N. Christlieb[2], P.C. Clark[13,6], S.C.O. Glover[6], F. Hammer[1], A. Koch[2], L. Monaco[14,15], L. Sbordone[16,17], and M. Steffen[18,1]

[1] GEPI, Observatoire de Paris, PSL Resarch University, CNRS, Univ Paris Diderot, Sorbonne Paris Cité, Place Jules Janssen, 92195 Meudon, France
[2] Zentrum für Astronomie der Universität Heidelberg, Landessternwarte, Königstuhl 12, 69117 Heidelberg, Germany
[3] Istituto Nazionale di Astrofisica, Osservatorio Astronomico di Roma, via Frascati 33, I-00040 Roma, Italy
[4] Kavli Institute for the Physics and Mathematics of the Universe, Todai Institutes for Advanced Study, The University of Tokyo, Kashiwa 277-8583, Japan
[5] Istituto Nazionale di Astrofisica, Istituto di Astrofisica Spaziale e Fisica Cosmica, Via Fosso del Cavaliere 100, I-00133 Roma, Italy
[6] Zentrum für Astronomie der Universität Heidelberg, Institut für Theoretische Astrophysik, Albert-Ueberle-Straße 2, 69120 Heidelberg, Germany
[7] Kavli Institute for Particle Astrophysics and Cosmology, Stanford University, SLAC National Accelerator Laboratory, Menlo Park, CA 94025, USA
[8] Department of Astronomy and Astrophysics, University of California, 1156 High Street, Santa Cruz, CA 95064, USA
[9] UPJV, Université de Picardie Jules Verne, 33 Rue St Leu, F-80080 Amiens
[10] Istituto Nazionale di Astrofisica, Osservatorio Astronomico di Trieste, Via Tiepolo 11, I-34143 Trieste, Italy
[11] Istituto Nazionale di Astrofisica, Osservatorio Astronomico di Padova Vicolo dell'Osservatorio 5, 35122 Padova, Italy
[12] Laboratoire Univers et Particules de Montpellier, LUPM, Université Montpellier, CNRS, 34095 Montpellier cedex 5, France
[13] School of Physics and Astronomy, The Parade, Cardiff University, Cardiff, CF24 3AA
[14] European Southern Observatory, Casilla 19001, Santiago, Chile
[15] Departamento de Ciencias Físicas, Universidad Andrés Bello, República 220, 837-0134 Santiago, Chile
[16] Millennium Institute of Astrophysics, Vicuña MacKenna 4860, Macul, Santiago, Chile
[17] Pontificia Universidad Católica de Chile Vicuña MacKenna 4860, Macul, Santiago, Chile
[18] Leibniz-Institut für Astrophysik Potsdam (AIP), An der Sternwarte 16, 14482 Potsdam, Germany

May 15, 2018

ABSTRACT

Context. In the course of the TOPoS (Turn Off Primordial Stars) survey, aimed at discovering the lowest metallicity stars, we have found several carbon-enhanced metal-poor (CEMP) stars. These stars are very common among the stars of extremely low metallicity and provide important clues to the star formation processes. We here present our analysis of six CEMP stars.
Aims. We want to provide the most complete chemical inventory for these six stars in order to constrain the nucleosynthesis processes responsible for the abundance patterns.
Methods. We analyse both X-Shooter and UVES spectra acquired at the VLT. We used a traditional abundance analysis based on OSMARCS 1D Local Thermodynamic Equilibrium (LTE) model atmospheres and the `turbospectrum` line formation code.
Results. Calcium and carbon are the only elements that can be measured in all six stars. The range is $-5.0 \leq$[Ca/H]< -2.1 and $7.12 \leq$A(C)≤ 8.65. For star SDSS J1742+2531 we were able to detect three Fe I lines from which we deduced [Fe/H] = −4.80, from four Ca II lines we derived [Ca/H]=–4.56, and from synthesis of the G-band we derived A(C)=7.26. For SDSS J1035+0641 we were not able to detect any iron lines, yet we could place a robust (3σ) upper limit of [Fe/H] < -5.0 and measure the Ca abundance, with [Ca/H]=–5.0, and carbon, A(C)=6.90, suggesting that this star could be even more metal-poor than SDSS J1742+2531. This makes these two stars the seventh and eighth stars known so far with [Fe/H] < -4.5, usually termed ultra-iron-poor (UIP) stars. No lithium is detected in the spectrum of SDSS J1742+2531 or SDSS J1035+0641, which implies a robust upper limit of A(Li)$<$ 1.8 for both stars.
Conclusions. Our measured carbon abundances confirm the bimodal distribution of carbon in CEMP stars, identifying a *high-carbon band* and a *low-carbon band*. We propose an interpretation of this bimodality according to which the stars on the *high-carbon band* are the result of mass transfer from an AGB companion, while the stars on the *low-carbon band* are genuine fossil records of a gas cloud that has also been enriched by a faint supernova (SN) providing carbon and the lighter elements. The abundance pattern of the UIP stars shows a large star-to-star scatter in the [X/Ca] ratios for all elements up to aluminium (up to 1 dex), but this scatter drops for heavier elements and is at most of the order of a factor of two. We propose that this can be explained if these stars are formed from gas that has been chemically enriched by several SNe, that produce the roughly constant [X/Ca] ratios for the heavier elements, and in some cases the gas has also been polluted by the ejecta of a faint SN that contributes the lighter elements in variable amounts. The absence of lithium in three of the four known unevolved UIP stars can be explained by a dominant role of fragmentation in the formation of these stars. This would result either in a destruction of lithium in the pre-main-sequence phase, through rotational mixing or to a lack of lateaccretion from a reservoir of fresh gas. The phenomenon should have varying degrees of efficiency.

Key words. Stars: Population II - Stars: abundances - Galaxy: abundances - Galaxy: formation - Galaxy: halo

1. Introduction

Carbon-enhanced stars are the most common objects in the extremely iron-poor regime. Very few stars with iron abundance below 1/10 000 do not show an over-abundance of carbon. They provide important clues that help understand the formation of the first low-mass stars in the history of the Universe. A carbon-enhanced metal-poor (CEMP) star has traditionally been defined as a star having [C/Fe]> +1 (Beers & Christlieb 2005), although [C/Fe]≥ +0.7 has been used (e.g. Aoki et al. 2007; Carollo et al. 2012; Norris et al. 2013; Lee et al. 2013; Carollo et al. 2014; Skúladóttir et al. 2015). In our opinion the latter criterion should not be used, since it may lead to ambiguous classifications. In fact the mean carbon-to-iron ratio of turn-off extremely metal-poor stars is < [C/Fe] >= +0.45 ± 0.1 (Bonifacio et al. 2009). These definitions are always purely phenomenological, and are not based on any theoretical consideration. Ambiguity may arise for some very luminous giants that are expected to have decreased their C abundance owing to mixing with material processed through the CNO cycle (Skúladóttir et al. 2015). A further shortcoming of this definition is for stars for which Fe cannot be measured. However, in all practical cases the upper limit on [Fe/H] allows a lower limit on [C/Fe] to be derived which determines whether a star is a CEMP or not. For the time being there are no major controversies on which stars are to be considered CEMP, although there are some on DLAs.

The turn-off Primordial Stars Survey (TOPoS) (Caffau et al. 2013b) [1] is aimed at finding stars of extremely low metallicity extracted from candidates selected from spectra of the Sloan Digital Sky Survey (York et al. 2000; Yanny et al. 2009; Dawson et al. 2013), data releases 7, 8, and 9 (Abazajian et al. 2009; Aihara et al. 2011a,b; Ahn et al. 2012). Our targets are mainly the carbon-normal turn-off stars. However, in warm stars the G-band may not be prominent in the low-resolution SDSS spectra, even if the star is a CEMP. When observed at higher resolution these stars reveal their true nature. In some cases we deliberately targeted some CEMP stars of extremely low metallicity in order to gain some further insight on the properties of these stars.

CEMP stars can be rich in heavy elements, which are normally built by both the "s-" and "r- processes". In this case they are called CEMP-rs stars, although the nucleosynthetic origin of the neutron capture elements in these stars is not very clear. It may in fact be more complex than a simple superposition of "normal" s- and r-processes (see Masseron et al. 2010, for a discussion); if they are rich only in heavy elements built by the s-process they are denominated CEMP-s. CEMP stars with a normal pattern of the heavy elements are called CEMP-no stars (see e.g. Beers & Christlieb 2005). The prototypical CEMP-no star is CS 22957-027 (Norris et al. 1997b; Bonifacio et al. 1998, with [Fe/H] = −3.43, A(C)=7.13). It is difficult to derive the chemical content of heavy elements in unevolved stars, and even more in the case of low- and medium-resolution spectra. In the present sample two stars can be classified as CEMP-rs (SDSS J1137+2553) and CEMP-s (SDSS J1245-0738) on the basis of their Ba abundance, following Masseron et al. (2010).

An interesting issue is the lithium abundance in unevolved CEMP stars compared to carbon-normal unevolved stars. Spite & Spite (1982) discovered that the warm metal-poor unevolved stars share a common lithium abundance, independent of effective temperature or metallicity. This is referred to as the *Spite plateau*. The unevolved CEMP stars usually display lithium abundances that are lower than the *Spite plateau*, although some of them do lie on the *Spite plateau*. Given that lithium is destroyed at temperatures higher than 2.5×10^6 K, the presence or absence of lithium and its precise abundance place strong constraints on the temperatures experienced by the material present in the stellar atmospheres and on possible lithium production events.

The bulk of the metals observed in stars has been produced by supernovae. The properties of CEMP stars can provide evidence of the existence and possible role of faint supernovae. A faint supernova is a core-collapse supernova such that its kinetic energy is of the order of a few 10^{50} erg, the velocity of the ejecta ≤ 1000 km s^{-1}, and the mass of ^{56}Ni of the order of a few 10^{-3} $M_\odot$. In such an explosion only the upper layers, rich in lighter elements (up to magnesium), are ejected and recycled in the interstellar medium. The deeper layers, rich in iron and heavier elements, fall back onto the compact object and do not contribute to the enrichment of the interstellar medium (see e.g. Ishigaki et al. 2014a, and references therein).

In this paper we present abundance determinations for six extremely iron-poor CEMP stars of which four are studied here for the first time. SDSS J1742+2531 was already analysed on the basis of an X-Shooter spectrum by Caffau et al. (2013a). In that paper we were able to provide the abundance of C, from the G-band and of Ca, from the Ca II K line. No lines of Fe, or any other element were detectable on that spectrum. In this paper we give an account of our further observations of this star conducted with UVES and providing higher resolution and S/N spectra. Star SDSS J1245-0738 has already been studied by Aoki et al. (2013).

2. Observations and data reduction

The coordinates and SDSS photometry of our programme stars are summarised in Table 1.

2.1. SDSS J0212+0137

For the star SDSS J0212+0137 we have nine 3000 s and two 3700 s exposures taken with UVES in the 437+760 nm setting, collected between August 6 and August 31, 2013. The slit width was set to 1.″4 to minimise the light losses, and the binning 2×2. In this case the resolving power was set by the seeing and since most observations were taken with a seeing around 1″ on the coadded spectrum, it is of the order of 47 000. The spectra were reduced in the standard way using the UVES pipeline (Ballester et al. 2000) within the ESO Common Pipeline Library. The radial velocity was measured on each individual spectrum and then spectra obtained on the same day were coadded and the radial velocity measured from this coadded spectrum. In both cases it was apparent that the radial velocity varied nearly linearly over the observation period. Both the radial velocities from the individual spectra and the daily means are given in Table 2. The line-to-line scatter in the velocities of each individual spectrum was typically less than 1 km s^{-1}and always less than 1.4 km s^{-1}. For comparison the SDSS radial velocity for this star is –2.7±3km s^{-1}, the spectrum was taken on the 27-09-2009, MJD

⋆ Based on observations obtained at ESO Paranal Observatory, programme 091.D-0288, 091.D-0305, 189.D-0165.

⋆⋆ MERAC Fellow

[1] The TOPoS survey is based mainly on ESO Large Programme 189.D-0165, and also on the precursor pilot programme conducted during the French and Italian X-Shooter guaranteed time, and on some normal ESO observing programmes conducted with UVES such as 091.D-0288 and 091.D-0305.

Table 1. Coordinates and magnitudes from SDSS

SDSS ID	RA J2000.0	Dec J2000.0	l deg	b deg	*u* [mag]	*g* [mag]	*r* [mag]	*i* [mag]	*z* [mag]	E(B–V) [mag]
SDSS J0212+0137	02 12 38.48	+01 37 58.08	160.37835821	−55.22255068	18.32	17.46	17.22	17.12	17.09	0.032
SDSS J0929+0238	09 29 12.33	+02 38 17.00	230.78095136	35.85905110	19.27	18.36	17.96	17.78	17.73	0.061
SDSS J1035+0641	10 35 56.11	+06 41 43.97	239.11776469	51.90944644	19.53	18.65	18.37	18.31	18.26	0.028
SDSS J1137+2553	11 37 23.26	+25 53 54.30	174.34692383	25.89841652	17.35	16.47	16.21	16.12	16.11	0.022
SDSS J1245–0738[a]	12 45 02.68	-07 38 47.10	191.26116943	−7.64641666	17.27	16.31	16.02	15.91	15.86	0.026
SDSS J1742+2531[b]	17 42 59.68	+25 31 35.90	49.85799222	25.64468718	20.06	18.91	18.67	18.55	18.49	0.065

[a] already studied by Aoki et al. (2013)
[b] already studied by Caffau et al. (2013a)

5502. Further monitoring of the radial velocity of this star is encouraged. The coadded spectrum has S/N = 79 at 392 nm, 87 at 450 nm, 134 at 670 nm, and 210 at 850 nm.

2.2. SDSS J0929+0238

SDSS J0929+0238 was observed with X-Shooter on May 12, 2013, for an exposure time of 3000 s in the IFU mode. The S/N is about 20 at 400 nm. Both the X-Shooter spectrum and the low-resolution spectrum of SDSS show an obvious G-band (see Fig. 1), and the star was targeted for this reason as well as for the very weak Ca II K line (see Fig. 2). This line and the G-band are the only metallic features we can detect from the X-Shooter spectrum; they provide only upper limits for iron and other elements. The radial velocity as measured from the Ca II K line is +398 km s^{-1} with an error estimate of 10 km s^{-1}. This is considerably lower than the velocity estimate of SDSS (+467 km s^{-1}± 10 km s^{-1}). However, considering that the SDSS measurement can rely only on the Balmer lines, unsuitable for accurate radial velocity measurements owing to their breadth (see e.g. González Hernández et al. 2008), it may well be that the error in the SDSS measurement is much larger than its formal estimate and thus the two radial velocities are consistent. It would nevertheless be interesting to monitor the radial velocity of this star since the difference between our measurement and the SDSS may indicate the presence of radial velocity variations.

2.3. SDSS J1035+0641

SDSS J1035+0641 was observed with X-Shooter on April 30 and May 1, 2013, on each occasion for an exposure time of 3000 s in the IFU mode. The S/N of the coadded spectrum is about 35 at 400 nm. No metallic features are detectable in our spectrum except for the Ca II K and H lines and the G-band. The radial velocities measured from the Ca II K line are -85 km s^{-1}and -70 km s^{-1}, with an estimated error of 10 km s^{-1}, thus making the two radial velocities consistent within 1σ. The SDSS radial velocity estimate is -47 km s^{-1}± 6 km s^{-1}, the same caveats apply here as discussed for SDSS J0929+0238, and we cannot be sure that this difference is real.

We also observed the star with UVES in service mode between February and April 2014 in the standard setting 390+580 nm. The slit was set to 1.″4 and the CCD binned 2 × 2, providing a resolving power $R \sim 32\,000$. Eleven observing blocks, each for an exposure of 3005 s, which were executed for a total time on target of about 9.2 hours. The reduced data was retrieved from the ESO archive. The median S/N of the individual spectra ranges from 3 to 6 in the blue. This makes it very difficult to measure the radial velocities on the individual spectra since we have to rely only on the Balmer lines. These rough measurements showed that the radial velocity of the different spectra was constant to within ±5 km s^{-1}. We therefore decided to coadd the spectra, after applying the appropriate barycentric correction to each one. The S/N ratio of the coadded spectrum is about 19 at 400 nm and 40 at 670 nm. The radial velocity measured on the coadded spectrum is -70.2 km s^{-1}with an estimated error of 2 km s^{-1}, which is consistent with the value from the X-Shooter spectra taken in 2013.

2.4. SDSS J1137+2553

For star SDSS J1137+2553 we have a single UVES spectrum of 3005 s observed on July 2, 2013, with the same set-up used for the observations of SDSS J0212+0137. The seeing was 1.″1. The spectrum has S/N=30 at 405 nm. The radial velocity measured from this spectrum is 137.7 ± 0.4 km s^{-1}in excellent agreement with the value from the SDSS spectrum (138.8 ± 3 km s^{-1}).

2.5. SDSS J1245-0738

For star SDSS J1245-0738 we have a single UVES spectrum of 972 s observed on May 9, 2013, with the same setup used for SDSS J0212+0137 and SDSS J1137+2553. The seeing was 1.″2. The spectrum is of poor quality and attains S/N=8 at 405 nm. In order to analyse it we smoothed it by rebinning it by a factor of 3 and this was sufficient to allow us to measure several metallic lines. The radial velocity measured from this spectrum is 77.7 ± 1.27 km s^{-1}, in excellent agreement with the measurement from the SDSS spectrum (75 ± 4 km s^{-1}). The star was also studied by Aoki et al. (2013) using a 20 minutes Subaru spectrum taken on March 10, 2008. Their measured radial velocity was +76.88 ±0.27 km s^{-1}; this is again in agreement with our measured radial velocity.

2.6. SDSS J1742+2531

SDSS J1742+2531 was observed with UVES at the VLT-Kueyen telescope in service mode, between April 17 and August 6, 2013. Altogether a total of 29 observing blocks of 3000 s exposure each were executed, 14 in the setting 390+580 nm and 15 in the setting 437+760 nm. One of the frames in the 390+580 nm setting had no useful signal. Our analysis is therefore based on the remaining 28 observing blocks. The projected slit on the sky was 1.″0, and the CCD was binned 1 × 1, providing a resolving

Table 2. Barycentric radial velocities for SDSS J0212+0137

Date	V_{bary} km s^{-1}	JD - 2400000.5 days
2013-08-06-01.279	2.39	56510.378487
2013-08-06-04.208	3.44	56510.271576
2013-08-06-22.838	3.67	56510.307209
2013-08-06-43.988	3.48	56510.342870
2013-08-12-13.675	3.87	56516.372381
2013-08-12-36.536	3.26	56516.253895
2013-08-12-46.360	3.36	56516.298453
2013-08-12-52.547	2.77	56516.335330
2013-08-13-10.375	3.71	56517.369565
2013-08-31-18.454	3.98	56535.273130
2013-08-31-39.166	5.73	56535.235870
Daily mean velocities		
2013-08-06	3.36 ± 0.53	56510.325000
2013-08-12	3.48 ± 0.52	56516.315000
2013-08-13	3.71 ± 0.55	56517.369565
2013-08-31	5.32 ± 0.65	56535.118070

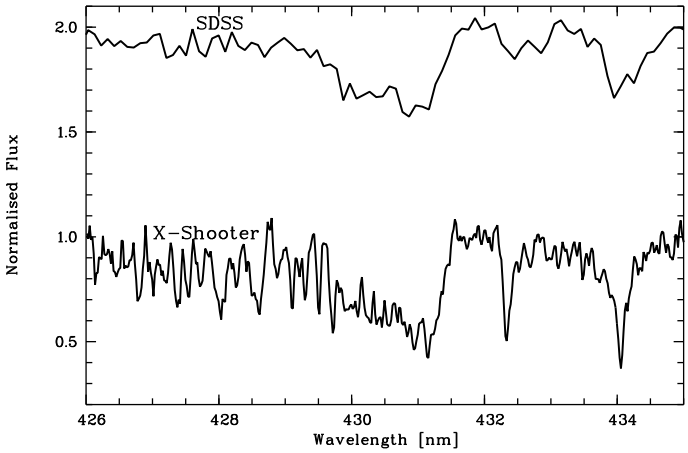

Fig. 1. SDSS J0929+0238, the G-band in the SDSS and X-Shooter spectra.

power of about 47 000. The spectra have been reduced using the UVES pipeline in the same way as those of SDSS J0212+0137. After performing the barycentric corrections all the individual spectra appeared to be at the same radial velocity, to better than 0.5 km s^{-1}. We therefore coadded all the 28 spectra in the intervals common to the two settings: 376-452 nm and 583-680 nm. In the range 328-376 nm we coadded the 13 spectra of the setting 390+580 nm and in the range 680-946 nm the spectra of the setting 437+760 nm. The S/N ratio of the coadded spectra is 3 at 336 nm, 20 at 382 nm, 23 at 450 nm, 44 at 518 nm, 45 at 670 nm and 36 at 850 nm. The measurement of the radial velocity is not trivial with so few detected lines. We obtained a first estimate of the radial velocity from the cores of the Balmer lines, and then refined it using the measured central wavelength of the seven detected metallic lines, the resulting radial velocity is −207.5 km s^{-1}±0.5 km s^{-1}(r.m.s.). This agrees with the SDSS radial velocity (−221 km s^{-1}±11 km s^{-1}) within 1.2σ.

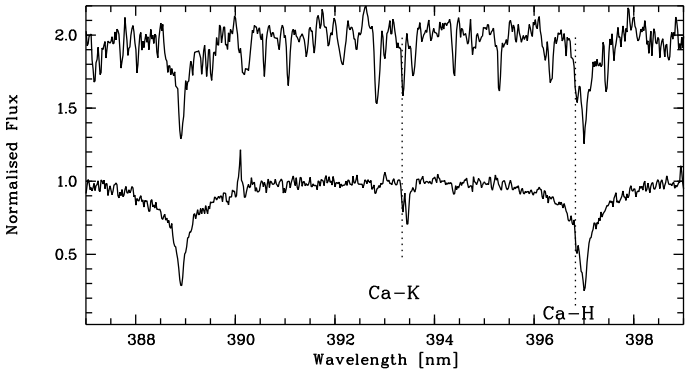

Fig. 2. The X-Shooter spectra around the Ca II H & K lines of SDSS J0929+0238 (the spectrum is vertically displaced by 1 unit for display purposes) and SDSS J1035+0641. The dotted lines mark the position of the stellar Ca II H &K lines. The CH lines are much more prominent in the former because the carbon abundance is almost 1 dex larger and the effective temperature is almost 300 K cooler.

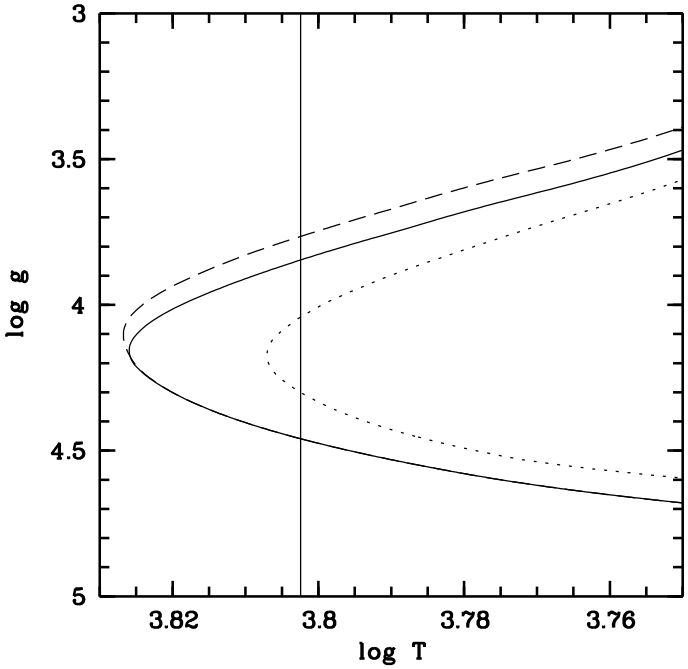

Fig. 3. Isochrones computed with the FRANEC code for 14 Gyrs and $Z = 2\times10^{-6}$ (dashed line), $Z = 2\times10^{-5}$ (solid line) and $Z = 2\times10^{-4}$ (dotted line). The vertical line marks our adopted $T_{\rm eff}$ for SDSS J1742+2531.

Table 3. Atmospheric parameters

SDSS ID	$T_{\rm eff}$ K	log g^a c.g.s	ξ^b km s^{-1}	[Fe/H]	[Ca/H]	A(C)
SDSS J0212+0137	6333	4.0	1.3	−3.59	−2.81	7.12
SDSS J0929+0238	5894	3.7	1.5	< −3.81	−4.02	7.70
SDSS J1035+0641	6262	4.0	1.5	< −5.07	−5.00	6.90
SDSS J1137+2553	6310	3.2	1.5	−2.70	−2.18	8.60
SDSS J1245-0738	6110	2.5	3.0	−3.21	−2.35	8.65
SDSS J1742+2531	6345	4.0	1.5	−4.80	−4.56	7.26

[a] logarithm of the gravitational acceleration at the surface of the stars expressed in cm s^{-2}
[b] microturbulent velocity

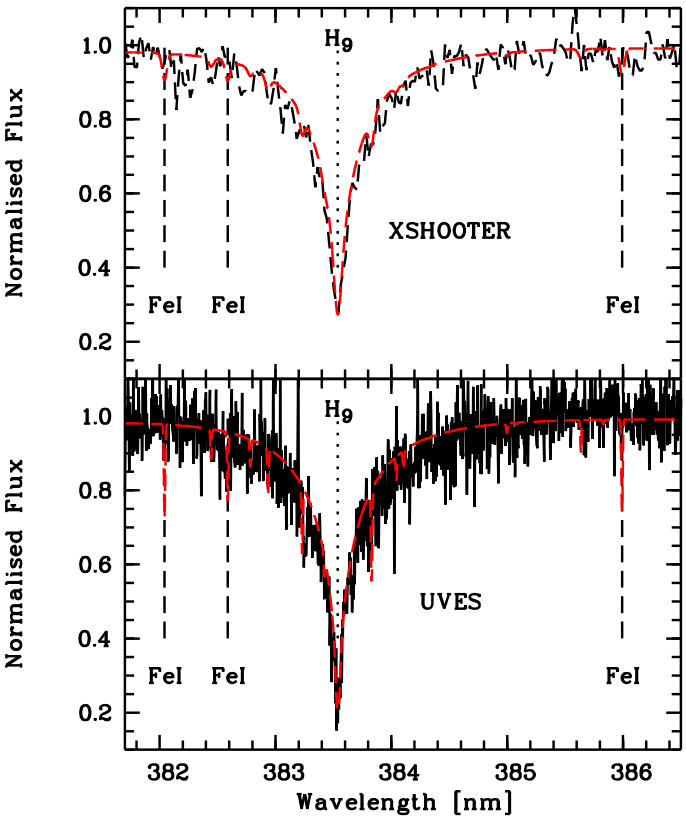

Fig. 4. SDSS J1035+06411: the X-Shooter (top panel) and UVES (bottom panel) spectra in the region covering the three strongest Fe I lines. The comparison spectrum is a synthetic spectrum computed with [Fe/H]=–4.5.

3. Analysis and results

3.1. Atmospheric parameters

The adopted atmospheric parameters for the programme stars are summarised in Table 3.

3.1.1. SDSS J0212+0137

For SDSS J0212+0137, we derived the temperature of 6333 K from the $(g-z)$ colour Ludwig et al. (2008), with an extinction of E$(g-z)$=0.07. The adopted gravity was log g=4.0, that achieves the iron ionisation equilibrium, although only one Fe II line could be measured. The effective temperature of this star is very near to that of SDSS J1742+2531, discussed later in this section, as is its global metallicity, dominated by the carbon (and presumed oxygen) overabundance with respect to iron. Thus the same isochrone is representative both for SDSS J0212+0137 and SDSS J1742+2531, and log g= 4.0 is appropriate for this $T_{\rm eff}$. For this star we exclude an RR Lyr nature; the observed radial velocity variations are not large enough and in any case we do not expect to observe a nearly linear variation of the radial velocity as shown in Table 2.

3.1.2. SDSS J0929+0238

For SDSS J0929+0238 we adopted a temperature of 5894 K, derived from the $(g-z)$ calibration. This temperature involves a gravity from isochrones of log g=4.5 or 3.7. We prefer the lower value of gravity as it provides a temperature from the wings of Hα consistent with the photometric value.

3.1.3. SDSS J1035+0641

For SDSS J1035+0641 we adopted a temperature of 6262 K, derived from the $(g-z)$ calibration. We used the same FRANEC isochrones described below in Sect. 3.1.5 to estimate the surface gravity, given the effective temperature. If the star is slightly evolved it has log g = 4.0, while if it is still on the main sequence it should have log g = 4.4.

3.1.4. SDSS J1137+2553 and SDSS J1245-0738

Also for SDSS J1137+2553 and SDSS J1245-0738 we adopted the effective temperature derived from the $g-z$ calibration that appears to be consistent with the wings of Hα and the iron excitation equilibrium. The gravity was derived by requiring the iron ionisation balance, to within the available uncertainty. These imply that SDSS J1137+2553 is a subgiant star and SDSS J1245-0738 is an HB star. The latter should be further monitored photometrically to check if it is an RR-Lyr. In the case it were an RR-Lyr our photometric temperature may be inadequate to describe our available spectrum. We note however that the lack of any radial velocity variation between our observation, that of Aoki et al. (2013) and the SDSS does not support an RR-Lyr status. Our adopted atmospheric temperature is very close to that adopted by Aoki et al. (2013, $T_{\rm eff}$= 6108 K) while we differ on the surface gravity. Aoki et al. (2013) *assumed* their stars to be turn-off without requiring the iron ionisation balance.

3.1.5. SDSS J1742+2531

For SDSS J1742+2531, in Caffau et al. (2013a) we adopted an effective temperature of 6345 K deduced from the $(g-z)_0$ colour and consistent with the wings of Hα from our X-Shooter spectrum. The wings of Hα from the UVES spectrum are also consistent with this temperature. We adopted log g = 4.0 for the surface gravity, that is appropriate for a metal-poor TO star of this effective temperature. In Fig. 3 we show a comparison with two isochrones computed with the FRANEC code (Chieffi, Limongi - private communication) for 14 Gyr, $Z = 2\times10^{-4}$ (dotted line), $Z = 2\times10^{-5}$ (solid line) and $Z = 2\times10^{-6}$ (dashed line). In spite of its very low iron abundance ([Fe/H] = −4.8, see Table 10), due to its large carbon enhancement, SDSS J1742+2531 should have a metallicity $1.8\times10^{-4} \leq Z < 2.8\times10^{-4}$, depending on its actual oxygen abundance, where the upper limit is given in Table 10 and the lower limit corresponds to [O/Fe] = +0.4. Taking the isochrone $Z = 2\times10^{-4}$ as reference, we have two possible solutions for the surface gravity for our assumed $T_{\rm eff}$: log g= 4.0, if the star is evolved past the turn off (TO), or log g = 4.3 if the star has not yet reached the TO. In the absence of any reliable gravity indicator we assume log g = 4.0, since this implies a larger distance. Given the rarity of these stars we assume that it is more likely that we found one of the brighter members of this population. In the next section, we nevertheless provide also the abundances computed assuming the higher gravity.

A possible concern is that the star may be indeed a horizontal branch star. In this case, it could be an RR-Lyr. To check if the star is an RR Lyr we measured the radial velocities of the Ca II H and K lines on all our available spectra and we did not find any variations above 1km s^{-1}. The Hα line is also clearly detected in the individual spectra, yet given its broad nature the accuracy of

the radial velocities determined is inferior to that of the metallic lines. We inspected the Hα line in all the spectra and found no evidence of variations above 5 km s^{-1}nor of the presence of P-Cyg profiles. The radial velocity amplitudes expected for an RR Lyr star are larger than 50 km s^{-1} for metallic lines and larger than 100 km s^{-1} for Hα (Sesar 2012). The typical periods of RR Lyr stars are less than a day and they should be adequately sampled by our data set. We obtained a photometric series in the *r* band of about 2h length with the AFOSC camera at the 1.82m telescope of Cima Ekar (Asiago), and the magnitude of this star seems constant with an r.m.s. of 0.02 mag, compatible with the S/N of the images. We are obtaining also longer photometric series with the Schmidt telescope of the Asiago Observatory in the *r* band to check for variability on longer time scales. All this photometric data will be fully discussed elsewhere. At the time of writing, we have no evidence of RR-Lyr – like variability of this star.

By looking at the figure 1 of Sandage (2010) and estimating the (B-V)$_0$ of the star to be 0.39, from its $(g-r)_0$ colour[2] we see that, as long as the absolute magnitude of the star is less than roughly 0.8, it lies in the instability strip. The isochrone shown in Fig. 3 implies also that a subgiant star with log g = 3.3 has M_V=2.7, thus keeping it well out of the instability strip. Horizontal branch stars, of a temperature similar to that of SDSS J1742+2531, should have a gravity that is this low or even lower (see figure 3 of Hansen et al. 2011 using the evolutionary tracks of Cassisi et al. 2004), depending on the star's mass. Moreover as discussed below in Sect. 3.2.6, a gravity as low as log g = 3.3, would bring about a 0.2 dex discrepancy between the Ca II K line and the Ca II triplet, and lower surface gravities would increase this discrepancy.

3.2. Chemical Abundances

To derive abundances and upper limits either from the equivalent widths or using synthetic spectra and line-fitting we used `turbospectrum` (Alvarez & Plez 1998; Plez 2012). We based our analysis on MARCS 1D LTE (Local Thermodynamic Equilibrium) model atmosphere (Gustafsson et al. 2008), that were interpolated in the grid computed for the TOPoS survey (Caffau et al. 2013b) for the atmospheric parameters of each star. As solar abundances we adopted carbon, nitrogen, oxygen and iron from Caffau et al. (2011a), for the other elements Lodders et al. (2009). If too few iron lines were measured to allow the determination of the microturbulence we adopted 1.5 km s^{-1}as in Caffau et al. (2013a)

3.2.1. SDSS J0212+0137

The higher abundance in iron and other elements in SDSS J0212+0137, coupled with the good quality of the spectrum allows us to obtain an extensive chemical inventory. The line by line abundances are provided in Table 4 and the mean abundances are provided in Table 5. The Fe abundance is derived from 17 Fe I lines and of the 8 measured Fe II lines we retain only one, that has an equivalent width larger than 0.5 pm[3] and this line provides the same abundance as the mean of the 17 Fe I abundances for our adopted surface gravity log g = 3.7. We measure both Sr and Ba in this star and their abundance classifies unmistakably the star as a CEMP-no. Remarkably we measure also the lithium abundance in this star that places it on the *Spite plateau* (Spite & Spite 1982). This pattern is indeed similar to that of SDSS J1036+1212 (Behara et al. 2010), that is a CEMP-no/s [4], has a relatively low-carbon abundance and has a lithium abundance in agreement with the *Spite plateau*.

Table 5. Mean abundances of SDSS J0212+0137

Ion	A(X)	A(X)$\odot$	[X/H]	σ	N lines
Li I	2.04	1.03			1
O I	6.70	8.76	–2.06		3
Mg I	4.53	7.54	–3.01	0.08	3
Al I	2.31	6.47	–4.16	0.04	2
Si I	4.15	7.52	–3.37		1
Ca I	3.35	6.33	–2.98		1
Ca II H&K	3.52	6.33	–2.81		2
Ca II IR	3.93	6.33	–2.40		3
Sc II	0.00	3.10	–3.10		1
Ti II	1.99	4.90	–2.91	0.13	9
Cr I	2.09	5.64	–3.55		1
Fe I	3.93	7.52	–3.59	0.15	17
Co I	2.49	4.92	–2.43		1
Ni I	2.77	6.23	–3.46	0.07	2
Sr II	–0.91	2.92	–3.83	0.06	2
Ba II	–1.40	2.17	–3.57		1
Molecular bands					
C –CH (G-band)	7.12	8.50	–1.38		
N –CN (388nm)	≤6.90	7.86	≤–0.96		

3.2.2. SDSS J0929+0238

For SDSS J0929+0238 no metallic features could be safely identified in the X-Shooter spectrum, except for the Ca II-K line, which gives A(Ca)=2.3, and the G-band, that implies a strong enhancement in carbon, A(C)=7.7. A higher resolution spectrum is required to determine the iron abundance of this star. The C and Ca abundances as well as a few upper limits are given in Table 6.

3.2.3. SDSS J1035+0641

For this star we have at our disposal both the X-Shooter and UVES spectra. The SDSS spectrum of SDSS J1035+0641 shows no detectable G-band and the star was targeted for the weakness of its Ca II K line (see Fig. 2), yet the X-Shooter spectrum allows us to detect a definite G-band, that qualifies the star as CEMP star with A(C)=6.80. The analysis of the UVES spectrum yields A(C)=6.9, confirming the result from the X-Shooter spectrum. The only metallic features measurable on our spectra (both X-Shooter and UVES) are the Ca II H&K lines. In Table 7 we provide the abundances of Ca and C and several upper limits, both for the assumption log g = 4.0 and log g =4.4. The upper limits for Li, Mg, Fe, and Sr are derived from the UVES spectrum, while the limit on Ba relies only on the X-shooter spectrum, since the strongest Ba II resonance line is not covered by the UVES spectrum. In the discussion we assume the values corresponding to log g = 4.0, since we consider this option makes the star brighter and its discovery more likely. For log g = 4.0 the Ca abundance A(Ca)=1.35, corresponding to [Ca/H]=–5.0. In Fig. 4 we show the observed r spectra in a region covering three

[2] From Table 1 of Jester et al. (2005): B-V = 0.98 × $(g-r)$ + 0.22

[3] 1pm = 10^{-12}m

[4] A CEMP-no/s is a star with +0.5 < [Ba/Fe] < +1.0 (Sivarani et al. 2006).

Table 7. Abundances of SDSS J1035+0641

Atomic lines								
Ion	λ nm	χ eV	log gf	EW pm	A(X) log g = 4.0	A(X) log g = 4.4	$A(X)_{err}$	A(X)⊙
Li I	6707.761[a]	0.00	–0.009	< 1.80	< 1.1[b]	< 1.1[b]		1.03
Mg I	518.3604	2.72	–0.239	< 0.30	< 2.47	< 2.47		7.54
Ca II	393.3663	0.00	0.105	syn	1.35	1.53	0.10	6.33
Fe I	382.0425	0.86	0.119	< 0.57[c]	< 1.91	< 1.91		7.52
Fe I	382.0425	0.86	0.119	< 1.67[d]	< 2.45	< 2.45		7.52
Sr II	407.7709	0.00	0.167	< 0.50	< −1.80	< −1.67		2.92
Ba II	4554.029	0.00	0.170	< 3.30	< −0.49	< −0.38		2.17
Molecular bands								
element	molecule		band		A(X) log = 4.0	A(X) log = 4.4		A(X)⊙
C	CH		G-band		6.90	6.70		8.50

[a] We list the strongest line of the doublet.
[b] Derived from the EW and the fitting formula of Sbordone et al. (2010).
[c] 1 σ
[d] 3 σ

Table 6. Abundances of SDSS J092912+023817

Atomic lines							
Ion	λ nm	χ eV	log gf	EW pm	A(X)	$A(X)_{err}$	A(X)⊙
Li I	6707.761[a]	0.00	–0.009	< 7.50	< 2.5[b]		1.03
Mg I	518.3604	2.72	–0.239	< 7.50	< 4.10		7.54
Ca II	393.3663	0.00	0.105	syn	2.30	0.07	6.33
Fe I	382.0425	0.86	0.119	< 2.73[c]	< 2.38		7.52
Fe I	382.0425	0.86	0.119	< 8.91[d]	< 3.71		7.52
Sr II	407.7709	0.00	0.167	< 7.80	< 0.04		2.92
Ba II	4554.029	0.00	0.170	< 1.50	< 0.20		2.17
Molecular bands							
element	molecule		band		A(X)	A(X)⊙	
C	CH		G-band		7.70	8.50	

[a] We list the strongest line of the doublet.
[b] Derived from the EW and the fitting formula of Sbordone et al. (2010).
[c] 1 σ
[d] 3 σ

Table 8. Mean abundances of SDSS J1137+2553

Ion	A(X)	A(X)⊙	[X/H]	σ	N lines
Li I	2.26	1.03			1
O I	7.18	8.76	–1.58		3
Na I	6.20	6.30	–0.10		2
Mg I	6.17	7.54	–1.37	0.09	3
Al I	3.30	6.47	–3.17		1
Si I	5.10	7.52	–2.42		1
Ca I	4.20	6.33	–2.13		2
Ca II K	4.15	6.33	–2.18		1
Ca II IR	4.60	6.33	–1.73		1
Sc II	1.03	3.10	–2.07		1
Ti II	2.49	4.90	–2.41	0.21	11
Cr I	3.03	5.64	–2.61		1
Fe I	4.86	7.52	–2.66	0.17	43
Fe II	4.84	7.52	–2.68	0.22	6
Co I	2.97	4.92	–1.95		1
Ni I	3.35	6.23	–2.88	0.13	2
Sr II	1.50	2.92	–1.42	0.14	2
Ba II	2.31	2.17	+0.14	0.32	6
Molecular bands					
C –CH (G-band)	8.60	8.50	+0.10		
N –CN (388nm)	7.86	6.88	-0.98		

of the strongest Fe I lines and a synthetic spectrum corresponding to [Fe/H]=–4.5, none of the three lines can be confidently detected. This is one of the five most iron poor stars found so far. Observations at higher resolution and S/N ratio are needed to determine the iron abundance of this star. No Li is detected in this star, however our upper limit confirms that the star is below the *Spite plateau*. An observation of the Li region with higher S/N is highly desirable.

3.2.4. SDSS J1137+2553

In spite of the poor S/N ratio of the only spectrum available for this star, the high resolution and wide spectral coverage of the UVES spectrum produced an almost complete chemical inventory summarised in Table 8. The C abundance is essentially solar while the oxygen abundance is 1.6 dex below solar and the N abundance only 1 dex below solar. This star, with [Fe/H] = −2.70, is the most metal-rich star in the present sample. Sodium is remarkably enhanced with respect to iron, with essentially a solar abundance. Magnesium also appears to be strongly enhanced, about 1.5 dex more than iron. The Sr and Ba abundances measured in this star suggest that it should be classified as a CEMP-rs star, using the criterion of Masseron et al. (2010). Another remarkable feature of this star is its Li abundance, with A(Li)=2.26 it lies clearly on the *Spite plateau*, unlike the majority of CEMP dwarf stars where Li is not measured

Table 9. Mean abundances of SDSS J1245-0738

Ion	A(X)	A(X)⊙	[X/H]	σ	N lines
Na I	4.30	6.30	–2.00		2
Mg I	5.05	7.54	–2.49		2
Al I	3.10	6.47	–3.37		1
Si I	4.30	7.52	–3.22		1
Ca I	3.53	6.33	–2.80		2
Ca II H&K	3.98	6.33	–2.35		2
Ca II IR	4.20	6.33	–2.13		1
Ti II	2.10	4.90	–2.80	0.25	7
Fe I	4.27	7.52	–3.25	0.48	29
Fe II	4.42	7.52	–3.10	0.17	3
Sr II	–0.38	2.92	–3.30		2
Ba II	0.23	2.17	–1.94		2
Molecular bands					
C –CH (G-band)	8.65	8.50	+0.15		

or appears clearly below the *Spite plateau* (Sivarani et al. 2006; Behara et al. 2010).

3.2.5. SDSS J1245-0738

The quality of the available spectrum is very poor, yet with the rebinning we were able to detect many metallic lines and confidently measure the carbon abundance from the G-band. It was possible to measure the abundance of nine elements, given in Table 9, and in spite of the large line-to-line scatter we derived [Fe/H] = −3.21 from thirty Fe I lines. The carbon abundance is roughly solar in this star as well, and both Na and Mg are strongly enhanced with respect to iron. The Sr and Ba abundances allow us to classify the star as a CEMP-s star. Our conclusion on the CEMP-s nature of this star agrees with that of Aoki et al. (2013). For all the neutral atoms (Na, Mg, Fe) our results agree very well with the results of Aoki et al. (2013). Their Ca abundance closely agrees with the value we determine from the Ca II H and K lines; however, there are strong discrepancies in the abundances of C, Sr, and Ba, and to a lesser extent of Ti. These differences are due to the different gravity values adopted in the two studies, corresponding to the HB status that we prefer and the TO status preferred by Aoki et al. (2013); the ionised atomic species are sensitive to the adopted gravity and so is the G-band.

3.2.6. SDSS J1742+2531

In spite of the higher resolution of our UVES spectrum of SDSS J1742+2531 compared to the X-Shooter spectrum presented in Caffau et al. (2013a), we can confidently detect only five metallic lines in addition to Ca II H and K, which were also detected in the X-Shooter spectrum: the two strongest lines of the infrared Ca II triplet and three Fe I lines. These are listed in Table 10. We provide the abundances implied by our spectra both for log g = 4.0 and log g = 4.3.

The Ca abundance is very coherent among Ca II H and K and the Ca II IR triplet. The mean Ca abundance of all four of the available lines is ⟨A(Ca)⟩ = 1.77 with a line-to-line standard deviation of 0.03 dex. This corresponds to [Ca/H] = –4.56 and is consistent with the Ca abundance that we derived only from the Ca II H and K in the X-Shooter spectrum ([Ca/H]≤ −4.5; Caffau et al. 2013a). The Ca I 422.6 nm line is not detected. The departures from LTE of the Ca lines in metal-poor stars have been extensively discussed in the recent literature (Spite et al. 2012a; Korn et al. 2009; Mashonkina et al. 2007) and it is recognised that the effects on the Ca II H and K lines is very small, while it can be significant for the Ca II IR triplet.

The gravity sensitivity of the Ca II H and K lines and of the Ca II IR triplet is very different, the first two being essentially insensitive to gravity. We checked the effect of a gravity as low as log g = 3.3 on the Ca abundances, the mean Ca abundance derived from the Ca II H and K lines is lower by 0.04 dex, while that deduced from the Ca II IR triplet is 0.22 dex lower. This gives a discrepancy of the order of 0.2 dex between the two transitions. Although this would still be within the errors– the line-to-line scatter would rise to only 0.1 dex and the calcium abundance would fall to 1.63– we believe it points towards a turn-off gravity around log g = 4.0.

The iron abundance derived from the Fe I lines is also very consistent among the three lines and is [Fe/H] = −4.80 with a standard deviation of 0.07 dex.

The analysis of the G-band confirms the carbon abundance we derived from the X-Shooter spectrum (A(C)=7.4 Caffau et al. 2013a) within errors A(C)=7.26±0.2. The quality of the spectra is not high enough to place any constraint on the $^{12}C/^{13}C$ ratio. We inspected our spectra to see if we could place meaningful upper limits on other elements and we provide these in Table 10, the limit on the EWs corresponds to a 3σ detection and σ has been estimated from the Cayrel formula (Cayrel 1988). We were not able to place a meaningful limit on the nitrogen abundance either from the UV NH band at 336 nm or from the violet CN band at 388 nm, as these would require a much higher S/N than provided by our spectra.

The Li I resonance doublet at 670.7 nm is not detected; the Cayrel formula and the measured S/N ratio imply that its EW is less than 0.83 pm (3σ criterion). The upper limit on the Li abundance was derived from the fitting formula of Sbordone et al. (2010) providing the 3D NLTE Li abundance. The 1D LTE or NLTE estimate would differ by only 0.03 dex, thus it is irrelevant in the present context.

3.3. Error estimates

The observational material presented here is heterogeneous as far as resolving power and signal-to-noise ratio are concerned. It is therefore not simple to provide a consistent estimate of the errors for our abundances. For the stars for which several lines of a given element are measured we provide the standard deviation of the measurements and that can be taken as an estimate of the statistical error on the abundance. When several lines are measured and no σ is provided (e.g. the O I triplet or Ca II H&K lines), this means that the lines have been fitted together. In these cases we suggest taking the line-to-line scatter of the Fe I lines as an estimate of the error because the statistical error is linked to the signal-to-noise ratio of the spectra, Fe I lines are found over a large wavelength range, and we assume that our measured line-to-line scatter is dominated by the noise in the spectrum.

The situation is less clear for the stars for which only a few lines can be measured. For these stars for each measured line we provide an estimate of the error on the equivalent width derived from the Cayrel formula (Cayrel 1988) and the measured signal-to-noise ratio in the spectrum. From this estimate of the error on the equivalent width we also derive an estimate of the error on the abundance. For the Ca II H and K lines for which the abundance has been derived using line profile fitting, we estimate the

Table 10. Abundances of SDSS J1742+2531

Atomic lines									
Ion	λ nm	χ eV	log gf	EW pm	EW_{err} pm	A(X) log g = 4.0	A(X) log g = 4.3	$A(X)_{err}$	A(X)⊙
Li I	6707.761[a]	0.00	–0.009	< 0.83		< 1.8[b]	< 1.8[b]		1.03
O I	777.1941	9.15	0.369	< 1.00		< 6.92	< 6.97		8.76
Na I	588.9951	0.00	0.117	< 0.90		< 2.14	< 2.14		6.30
Mg I	518.3604	2.72	–0.239	< 1.00		< 3.07	< 3.07		7.54
Si I	390.5523	1.91	–1.041	syn		< 3.05	< 3.05		7.42
S I	921.2863	6.53	0.420	< 1.10		< 4.61	< 4.75		7.16
Ca I	422.6728	0.00	0.265	< 1.00		< 1.62	< 1.62		6.33
Ca II	393.3663	0.00	0.105	syn		1.79	1.81	0.04	6.33
Ca II	396.8469	0.00	–0.200	syn		1.76	1.79	0.08	6.33
Ca II	854.2091	1.70	–0.514	6.20	0.29	1.72	1.81	0.05	6.33
Ca II	866.2141	1.69	–0.770	5.20	0.29	1.79	1.88	0.05	6.33
Fe I	382.0425	0.86	0.119	2.40	0.35	2.73	2.73	0.09	7.52
Fe I	382.5881	0.92	–0.037	1.90	0.35	2.80	2.80	0.09	7.52
Fe I	385.9911	0.00	–0.710	1.90	0.35	2.63	2.63	0.09	7.52
Sr II	407.7709	0.00	0.167	< 1.40		< −1.25	< −1.16	2.92	
Ba II	4554.029	0.00	0.170	< 1.50		< −0.97	< −0.84	2.17	

Molecular bands					
element	molecule	band	A(X) log = 4.0	A(X) log g = 4.3	A(X)⊙
C	CH	G-band	7.26	7.08	8.50

[a] We list the strongest line of the doublet.
[b] Derived from the EW and the fitting formula of Sbordone et al. (2010).

error as the corresponding diagonal element in the covariance matrix of the fit, ignoring all the off-diagonal terms.

For the carbon abundances (and nitrogen abundances from the CN band), the error is dominated by the placing of the continuum. Our fitting was limited to the blue part of the band, excluding the band-head. Given that the fit covers a large wavelength range, the error in the continuum placement is not dominated by the signal-to-noise ratio (the noise is averaged out over so many pixels, yet it does play a role), but rather by the quality of spectrum rectification (removal of the blaze function). In Spite et al. (2006) error estimates on the fitting of the G-band are provided, resulting from fits derived by fixing slightly different continuum levels. In that case the errors are of the order of 0.1 dex. In the present case the data are of much lower S/N ratio, and for the X-Shooter spectra resolving power as well. We estimate 0.15 dex, which is a conservative estimate of the error on our C abundances.

The systematic errors, i.e. the effect of the adopted atmospheric parameters on the derived abundances have often been discussed in the literature; we point to the reader Table 4 of Bonifacio et al. (2009) where this exercise is done for a star with atmospheric parameters close to the stars discussed in the present paper. The systematic errors in our case are of the same order of magnitude. In that table the systematic error on the C abundances derived from the G-band is not discussed: a change in temperature of 100 K corresponds to a change of 0.17 dex in C abundance.

3.4. Effects of departures from local thermodynamic equilibrium

The deviations from LTE in the formation of Ca I and Ca II lines in metal-poor stars has been extensively studied by Mashonkina et al. (2007) and Spite et al. (2012a). It has been recognised that the Ca I 422.6 nm resonance line provides discrepant results even when computed in NLTE (Spite et al. 2012a), for this reason we never used the abundance from this line even when it was measured. On the other hand, both Ca II K line and and the IR triplet lines can provide reliable Ca abundances. While the K line is always formed quite close to LTE conditions, the IR triplet shows significant deviations from LTE. The NLTE corrections are always negative. This can be appreciated in the three stars SDSS J0212+0137, SDSS J1137+2553, and SDSS J1245-0738. In all three stars the IR triplet provides Ca abundances that are higher by 0.2 to 0.4 dex than the K line. This is compatible with expected NLTE corrections. According to the computations of Mashonkina et al. (2007), at a metallicity of –3.0 for $T_{\rm eff}$ = 6000 and log g = 4.0 the non-LTE correction for the IR triplet is –0.23 dex. Star CS 29527-015, analysed by Spite et al. (2012a), has parameters very close to those of SDSS J0212+0137 and the computed NLTE correction is –0.51 dex.

The exception is SDSS J1742+2531, for which the LTE analysis provides the same Ca abundance from the H and K lines and from the IR triplet. Although the star has almost the same atmospheric parameters as the three above-mentioned stars, we note that its Ca abundance is much lower, thus the equivalent width of the IR triplet lines is smaller. Generally speaking, as the equivalent width of a line decreases it forms closer to LTE. Although we do not have in hand specific computations for the Ca II IR triplet to demonstrate this effect, we know it can be seen for other

lines (see e.g. Fig. 6 in Andrievsky et al. (2007) illustrating this behaviour for the Na I D lines). It is thus quite likely that the NLTE corrections for the IR Ca triplet in SDSS J1742+2531 are much smaller than for the other three stars

Regarding NLTE effects on neutral iron for star HE 1327-2326, Aoki et al. (2006) adopted a correction of +0.2 dex, based on several previous investigations (Gratton et al. 1999; Korn et al. 2003; Thévenin & Idiart 1999). This value should also be appropriate for SDSS J1742+2531, which has similar atmospheric parameters.

3.5. Effects of granulation

It is well known that the formation of molecular bands in the atmospheres of metal–poor stars is prone to strong granulation effects (see e.g. Bonifacio et al. 2013, and references therein). From Table 6 in Bonifacio et al. (2009) we estimate that a correction between –0.5 and –0.6 dex in the carbon abundance derived from the G-band is necessary for all the stars here investigated.

For the three lines of Fe I measured in SDSS J1742+2531, the 3D correction is about –0.4 dex, consistent with the Bonifacio et al. (2009) results. This implies that NLTE and granulation effects have opposite directions, and they may tend to cancel; however, for iron it is not possible to simply add the 3D and NLTE corrections (Mashonkina et al. 2013). The granulation effect for Ca II lines is small, of the order of –0.1 dex (Caffau et al. 2012).

4. On the carbon abundances in CEMP stars

Of the six stars analysed in the present paper, two – SDSS J1137+2553 and SDSS J1245-0738 – have been classified as CEMP-rs and CEMP-s, respectively. For the purposes of this discussion we consider these objects as a single class (CEMP-rs+CEMP-s), subdivided into two different subclasses (CEMP-s and CEMP-rs). As detailed below, there are reasons to believe these stars are the result of mass-transfer from an AGB companion in a binary system. For these two particular stars, this may be at odds with the lack of obvious radial velocity variations, yet few measurements are available. One cannot exclude the hypothesis that both systems are seen nearly face-on, hence with little or no radial velocity variations.

We now concentrate our discussion on the four other stars, of which SDSS J0212+0137 can be classified as a CEMP-no star. For the three other stars it is not possible to establish whether they are CEMP-s or CEMP-no on the basis of the abundances of Ba because the available upper limits do not allow us to distinguish between the two classes. However, as discussed in Sect. 4.1, on the basis of their carbon abundance we have reasons to believe that they are indeed CEMP-no stars.

An interesting feature displayed by the CEMP stars is shown in Fig. 5. There are many known CEMP stars with [Fe/H] > -3.5. If we plot the histogram of the carbon abundances in these stars, we see that the distribution is clearly bimodal (Fig. 5). Each of the two peaks is quite wide, almost one dex, but they appear to be rather well separated. In the following we shall refer to these two peaks in carbon abundance as the *high-carbon band* and the *low-carbon band*. Quite interestingly all stars with [Fe/H] < -3.5 belong to the *low-carbon band*. Another way to look at the carbon abundances is to plot the carbon abundance versus [Fe/H], as in Fig. 6. Similar plots have already been shown in Behara et al. (2010), Masseron et al. (2010), Spite et al. (2013) and Caffau et al. (2013a).

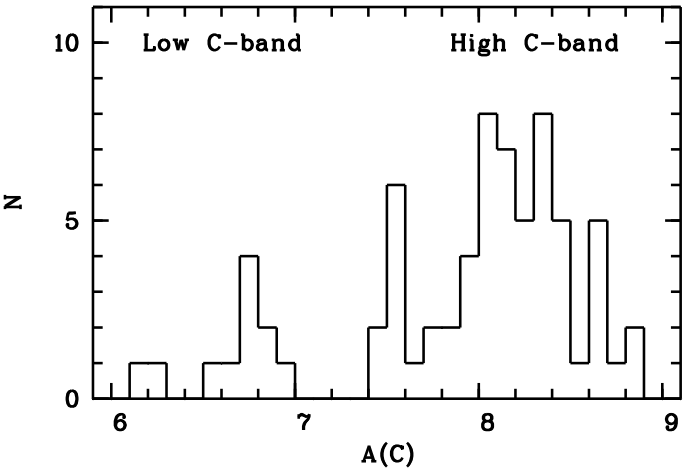

Fig. 5. Carbon abundances in all the CEMP stars in the present paper and in the literature with [Fe/H] > -3.5 (Sivarani et al. 2006; Thompson et al. 2008; Aoki et al. 2008; Behara et al. 2010; Placco et al. 2011; Carollo et al. 2012; Masseron et al. 2010, 2012; Yong et al. 2013; Cohen et al. 2013; Spite et al. 2013; Caffau et al. 2013a). The bimodal distribution is clear in this plot. We refer to the peak at lower carbon abundance as the *low-carbon band* and to the peak at higher carbon abundance as the *high-carbon band*.

In Fig. 6 we have included only unevolved stars since giant stars may be internally "mixed" (Spite et al. 2005, 2006) and the C abundance may thus be decreased by an amount that is generally difficult to estimate. We have included in the plot only stars from the literature that have a measured Ba abundance or a significant upper limit (Sivarani et al. 2006; Frebel et al. 2005, 2006; Thompson et al. 2008; Aoki et al. 2008; Behara et al. 2010; Masseron et al. 2010, 2012; Yong et al. 2013; Cohen et al. 2013; Li et al. 2015), so as to have some indication on their classification as CEMP-no, CEMP-s, or CEMP-rs. In order to clearly define the behaviour of the carbon abundance at low metallicity, we have also included the ultra-iron-poor subgiant HE 1327-2326 (Frebel et al. 2005, 2006; Cohen et al. 2013) and SDSS J1619+1705 (Caffau et al. 2013a), even though their Ba abundance is undetermined. We have also included the lower RGB giants SMSS J0313-6708 (Keller et al. 2014), HE 0107-5240 (Christlieb et al. 2004) and HE 0557-4840 (Norris et al. 2007), which are in the CEMP-no class. These stars are not more luminous than the RGB "bump" and therefore should not be deeply "mixed"; however, they have undergone the first dredge-up and following Bonifacio et al. (2009) their carbon abundance should have been lowered by 0.26 dex compared to any TO star.

The new determination of A(C) for SDSS J1742+2531, based on the UVES spectra, has replaced the earlier value based on X-Shooter. These new observations, especially that of SMSS J0313-6708, confirm that all the lowest metallicity stars belong to the *low-carbon band*. There is a wide scatter (over 1 dex) in carbon abundances among these stars, yet there is no clear trend with [Fe/H] and they are all well below the *high-carbon band* defined by the other CEMP stars, which is almost at solar C abundance. Here we redefine the class of CEMP-no stars as [Ba/Fe] ≤ 1.2. The limit of [Ba/Fe] = 1.2 was chosen because it is the highest value reached (LTE computation) by the normal metal-poor stars (not C-rich) (Hill et al. 2002; François et al. 2007; Spite et al. 2014). This new definition also has the virtue of allowing us to classify SDSS J1036+1212 and CS 29528-41 as CEMP-no; they had previously been classified as CEMP-no/s

and CEMP-s by Behara et al. (2010) and Sivarani et al. (2006), respectively. The new definition does not require a new class to be created for these two objects.

The vast majority (91%) of stars on the *high-carbon band* are of the type CEMP-s or CEMP-rs; this population of stars is compatible with a population of 100% binaries of shorter periods, at a maximum of 20 000 days (Starkenburg et al. 2014, see also Lucatello et al. 2005). The stars of the *low-carbon band* for which Sr and Ba have been measured are all of the CEMP-no type. Although two of them have been found to be binaries (Starkenburg et al. 2014), the binary frequency is similar to that observed in the solar neighbourhood. A very clear picture is emerging from the observations and we propose an interpretation.

4.1. High-carbon band

As a consequence of the results of Starkenburg et al. (2014) and Lucatello et al. (2005) on the binarity of the CEMP-s stars (100% of binaries), we assume that the *high-carbon band* CEMP stars are all post-mass transfer binary systems. The originally more massive star of the system has gone through the AGB phase and donated mass to its companion, and subsequently evolved to the present white dwarf status. The high-carbon abundances in these stars have three causes: *i)* the AGB stars enrich their atmospheres through the third dredge-up of carbon produced in the He-burning shell, the amount of carbon produced and dredged up is independent of the star's initial metallicity; *ii)* since the binary system is extremely metal-poor, once this material is transferred to the companion, the transferred carbon exceeds the carbon originally present in the companion's atmosphere by at least an order of magnitude (see Fig. 6), thus the metallicity of the system is again irrelevant with respect to the final carbon abundance in the companion; and *iii)* the dilution factor[5] varies over a limited range.

This last requirement is supported by the study of Bisterzo et al. (2011), who have analysed a sample of 100 CEMP-s stars for which detailed chemical abundances are available (almost all the stars that appear in Fig. 6 are in their sample) and showed that the abundances of light elements (C,N,O, Na, Mg) and neutron capture elements can be reproduced assuming transfer from an AGB star in the mass range 1.3-2 $M_\odot$ and logarithmic dilution factors in the range 0.0-2.5. This is consistent with the constraints deriving from the carbon abundance alone. The *high-carbon band* spans the range A(C)=7.4–8.9, the same range covered by the carbon abundances in the AGB donor, according to Table 6 of Bisterzo et al. (2010). The range of masses of the primary star is narrowed by the nucleosynthesis requirements; the mass of the secondary is even narrower. Observations indicate that they are all of spectral type F or G, which means, given the old age presumed from the low metallicity, they are in the mass range $0.7M_\odot$ to 0.9 $M_\odot$. The study of Masseron et al. (2010) also supports this point of view; they detect a strong correlation between Ba and C abundances in CEMP-s stars. They claim that this supports the operation of a ^{13}C neutron source in the AGB companions that are responsible for the C and *s*−process enrichment in the CEMP-s stars. The orbital parameters must also lie in a relatively narrow range to allow mass transfer to take place during the AGB phase of the primary. The result of Starkenburg et al. (2014) that the periods are all shorter than 20 000 days corroborates this hypothesis. We note that the study of Aoki et al. (2015) also suggests that the binary stars among extremely metal-poor stars are biased towards shorter periods.

This does not imply that binary systems are not created with a wide range of mass ratios and orbital parameters, but that only a subset of these systems may evolve in such a way as to give rise to a *high-carbon band* CEMP star. This follows from the results of Lucatello et al. (2005) and Starkenburg et al. (2014) on binarity and of Bisterzo et al. (2011) on nucleosynthesis.

This scenario also explains why such stars are not found at higher metallicities. In that case the carbon initially present in the secondary's atmosphere is non-negligible with respect to the amount transferred. As a consequence the star is not classified as carbon enhanced because the C/Fe ratio is not very high. It has already been pointed out that these CEMP-s systems are indeed low-metallicity analogues of CH stars and Ba stars (see Starkenburg et al. 2014, and references therein).

Our proposed scenario has interesting implications in the light of the results of some of the current simulations of Pop III star formation (Clark et al. 2011a; Smith et al. 2011; Greif et al. 2012; Dopcke et al. 2013; Stacy et al. 2013; Stacy & Bromm 2014). The above studies unanimously predict a very high binary fraction for Pop III stars and a wide mass range with some Pop III stars eventually undergoing the AGB stage. If such a star is formed in a binary system, it may transfer the metals produced in the AGB phase to the companion. None of the stars in the *high-carbon band* can be a Pop III star because there is no way an AGB star can enrich the companion in Fe. However, this is a motivation for searching for *high-carbon band* stars even at lower metallicity–to find some Fe-free stars. According to our proposed scenario SMSS J0313-6708 is not one of the Pop III stars that have accreted mass from an AGB companion because its C content is too low, unless extensive internal mixing has decreased the C abundance by about 1 dex to form N. This is, however, unlikely considering the surface gravity of the star (log g = 2.3).

4.2. Low-carbon band

We propose that these stars are not the result of transfer from a companion. Some of them may well be members of a binary system (Starkenburg et al. 2014), but no mass transfer has taken place. The atmospheric abundances of these stars are bona fide fossil records of the interstellar medium out of which they were formed. The variable carbon abundance displayed in these stars is the result of the nucleosynthesis of a few core collapse SN of zero metallicity that have polluted the gas. The variation in the carbon abundances reflects a range of masses in the SN progenitors, as well as varying degrees of dilution of the SN ejecta with primordial gas. The spread in Fe abundance reflects a spread in the amount of fall-back of the SN that produced the bulk of carbon.

None of these stars has yet been observed with a C abundance as high as the *high-carbon band*, which places constraints on the minimum dilution possible and the maximum C production by the SN that polluted the ISM. Only the product of these two quantities is constrained, however[6].

[5] Defined as the base 10 logarithm of the mass of the convective envelope of the star to the mass of material accreted by the AGB companion

[6] It is straightforward to pass from abundance in number in the usual spectroscopic notation A(X) to the mass concentration usually used by chemists: $M(X)/M(H) = 10^{(A(X)-12)} \times \frac{m_X}{m_H}$, where m_X and m_H are the atomic weights of element X and hydrogen, respectively. An abundance A(C)=6.80 corresponds to a mass concentration of $\sim 7.5 \times 10^{-5}$. This means that, for example, if a SN ejects a mass of 1 $M_\odot$ of carbon, this

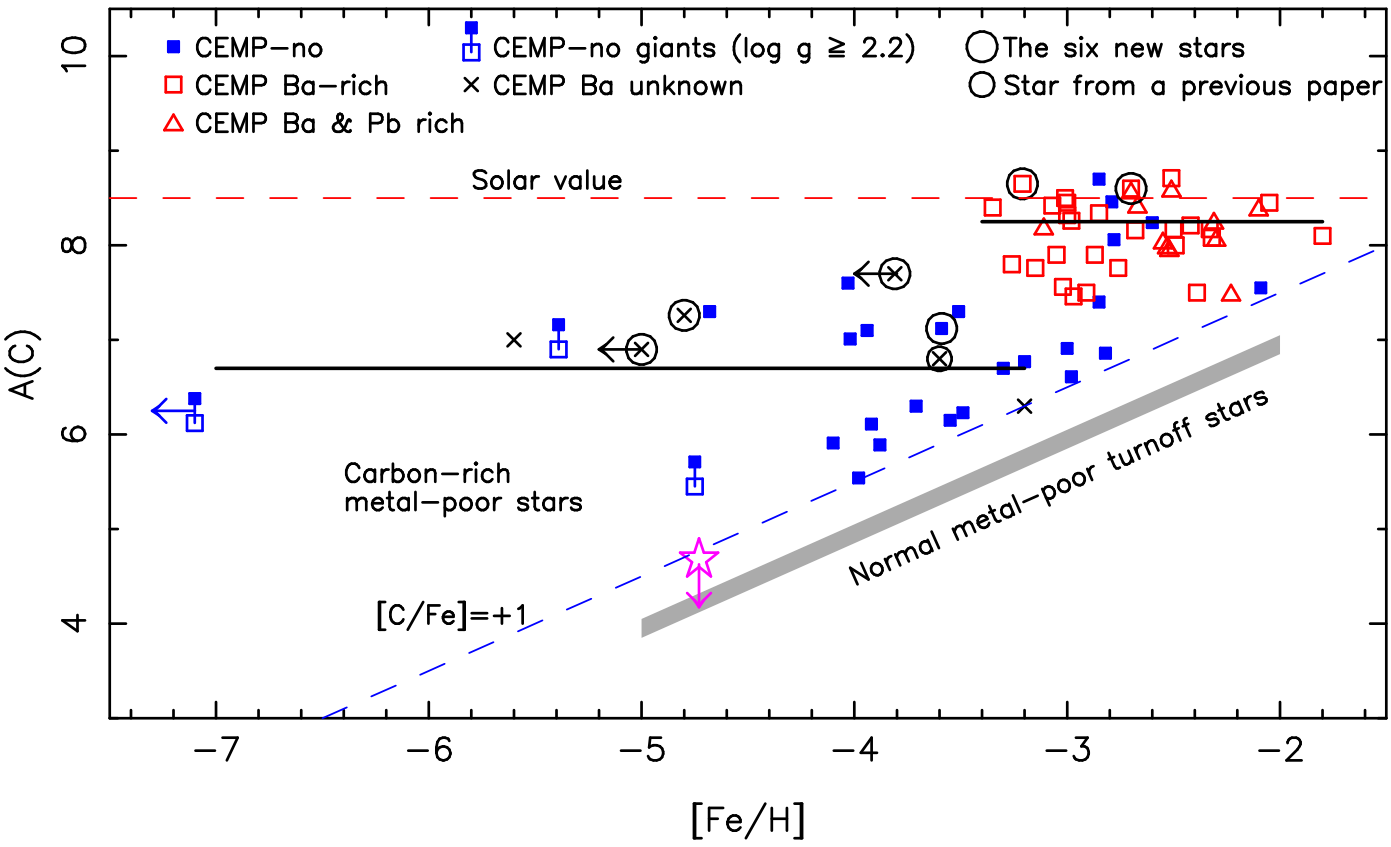

Fig. 6. The carbon abundances A(C) of CEMP stars as a function of [Fe/H]. The stars in the present paper and in Caffau et al. (2013a) are shown with big and small circles, respectively. The other turn-off stars come from the literature (Sivarani et al. 2006; Frebel et al. 2005, 2006; Thompson et al. 2008; Aoki et al. 2008; Behara et al. 2010; Masseron et al. 2010, 2012; Yong et al. 2013; Cohen et al. 2013; Li et al. 2015). The CEMP-no turn-off stars are represented by filled blue squares. The CEMP-no giants are represented by two symbols: an open blue square for the measured value of the C abundance, and a filled blue square for the empirically corrected (for the first dredge-up) A(C) value. The CEMP-s or -rs stars are indistinctly represented by open red squares, but by open red triangles if they are also Pb-rich. When the Ba abundance is unknown the star is marked with a black cross. The upper limit marked as a violet star is the only "C-normal" star that appears in this plot: SDSS J1029+1729 (Caffau et al. 2012). The solid horizontal (black) lines represent the mean value of the carbon abundance for CEMP stars with [Fe/H] > −3.0 (A(C)=8.25) and for CEMP stars with [Fe/H] < −3.4 (A(C)=6.8) as derived by Spite et al. (2013). On the upper A(C) band all the stars but four (HE 0007-1832, HE 022-4831, SDSS J0036-1043, and CS 22958-42) are Ba-rich. On the contrary, on the lower A(C) band all the stars are CEMP-no.

4.3. Carbon enhanced damped Lyα galaxies

We can use damped Lyα galaxies (DLAs) to determine detailed abundances at high redshift, and compare the results to the metal-poor stars in our Galaxy. Kulkarni et al. (2013) presented a model of chemical enrichment of galaxies, according to which high redshift galaxies with low-mass haloes ($M \lesssim 10^9$ $M_\odot$) are sensitive to the initial mass function (IMF) of Pop III stars. They tentatively identify such galaxies with DLAs. No absorption system as metal-poor as the most metal-poor Galactic stars has yet been found, the record holder being the Lyman limit system at $z = 3.410883$ towards QSO J1134+5742, for which no metallic lines could be detected; an upper limit on the metallicity of $Z < 10^{-4.2} Z_\odot$ has been determined (Fumagalli et al. 2011). However, there is a handful of DLA galaxies at [Fe/H] ~ -3.0 and for a few C abundances have also been measured. In particular, the $z = 2.30400972$ DLA towards QSO J0035-0918 with [Fe/H] = −3.09 (on our adopted solar abundance scale) has been claimed to be a CEMP system, in the sense that [C/Fe] > +1. The absolute C abundance measured by Cooke et al. (2011) is A(C)=6.92, corresponding to the previously defined *low-carbon band*. The measurement is very delicate because the C II lines are saturated and therefore the derived column density is very sensitive to the adopted turbulent velocity *b*. Carswell et al. (2012) revised the measurement, adopting a purely thermal model and derived A(C)=5.92. Dutta et al. (2014) also analysed this system, and their preferred model has a very low turbulence ($b = 0.89$ km s^{-1}) implying A(C)=5.90, but by adopting $b = 2.0$ km s^{-1} this value rises to A(C)=7.63. If the lower C abundances are adopted then the system no longer has [C/Fe] > +1. What is important for the present discussion is that all the proposed C abundances are essentially compatible with the *low-carbon band*, although the lower values are on the low side. We suggest that this is consistent with our scenario; this DLA galaxy should have been enriched by only a few zero-metallicity SNe, at least one of which must have been faint (see Sect. 5). Our scenario would be challenged if the carbon abundance had been found on the *high-carbon band*, since it is unlikely that a whole galaxy could be polluted essentially by AGB stars. There is another interesting system, the DLA at $z = 3.067295$ towards QSO J1358+6522 (Cooke et al. 2012) that has A(C)=6.18 and [Fe/H] = −2.89. Again this system is compatible with the *low-carbon band*. None of the known metal-poor DLAs shows a carbon abundance compatible with the *high-carbon band*. There are

has to be diluted with 1.33×10^4 $M_\odot$ of hydrogen in order to reach this mass concentration, or, equivalently, carbon abundance.

carbon-normal DLAs, that fall in the shadowed region in Fig. 6. It would be extremely important to detect other DLAs with metallicity as low as that observed in Galactic stars in order to compare the same metallicity regime.

There is another thing that is intriguing; the metal-poor halo stars for which ages can be measured always have ages in excess of 12 Gyr or even of 13 Gyr, which corresponds to a redshift in excess of 10. A redshift $z = 3$ corresponds to a look-back time of 11.5 Gyr. If our proposed scenario is correct, the two DLAs above have been forming zero-metallicity stars at very late times. This suggests that primordial gas clouds could exist and trigger star formation down to at least $z = 2.3$. A similar conclusion has been reached in a completely independent way by considering the low N/O ratios found in DLAs (Molaro et al. 2004; Zafar et al. 2014). We cannot exclude that the stars that enriched these DLAs actually formed 13 Gyr ago, and that the DLA galaxy has not undergone any star formation since. However, this seems very unlikely. The DLA systems have a high H column density (hence the damping wings on the Ly α line), comparable to that of the Milky Way disc if it were seen face-on. It is natural to assume that this also implies a high volume density, which should ensure ongoing star formation as in the Milky Way disc. If this is the case the SNe that have enriched the gas we are observing exploded less than 10^7 years earlier.

One cannot exclude that any given DLA is a long filament of low volume density seen along its length and that it hosts no star formation. This seems to be a very contrived hypothesis and may only apply to a small fraction of the observed DLAs given the difference in cross section of a gas filament and a star forming galaxy like the Milky Way or the Magellanic clouds. It would be very important to be able to find and study DLAs at higher z, which may be possible thanks to the IR capabilities of the next generation of 30 m class telescopes.

The high redshift DLAs at low metallicities can also provide us with some interesting insights into the presence of dust. We have been invoking dust as the main cooling agent and DLAs provide evidence for the presence of dust from the abundance ratios of volatile to refractory elements of similar nucleosynthetic origin, such as Zn/Fe or S/Si. The refractory elements are usually found to have lower abundances; however, Molaro (2006) noted from the Zn/Fe ratios that below [Fe/H] = −2 there seems to be no evidence of dust depletion, suggesting a lack of dust in the lowest metallicity DLAs. A similar result has been found by Rafelski et al. (2012) for the Cr/Zn ratios. It is interesting to note that in the $z = 3.067295$ DLA towards QSO J1358+6522 the ratio Si/S is essentially solar [Si/S] = 0.07±0.09 (Cooke et al. 2012). In the DLA at $z = 2.30400972$ towards QSO J0035-0918, the ratio Si/O is again solar, [Si/O]=+0.06 ± 0.14 (Dutta et al. 2014). Although these systems have a low dust content, it may still be sufficient to act as a coolant for the formation of low-mass stars. The existing studies of this topic (Schneider et al. 2006; Omukai et al. 2008; Dopcke et al. 2011; Schneider et al. 2012a; Dopcke et al. 2013) find that if one assumes that the dust-to-gas ratio D scales with the metallicity Z, one only needs a metallicity of the order of 10^{-5} solar to get effective dust cooling. This means that if we relax the assumption that D scales with Z, for example assuming a constant dust-to-gas ratio, we only need an absolute dust abundance of the order of 10^{-7} solar. In gas with gas-phase metallicity 10^{-3} solar, our required dust-to-metals ratio is therefore only 10^{-2}, and the associated elemental depletion would not be detectable given the current errors on the abundances. If we account for the fact that dust grains can grow during the gravitational collapse of the gas (see e.g. Chiaki et al. 2014), then our required initial dust abundance is even smaller and this argument is stronger.

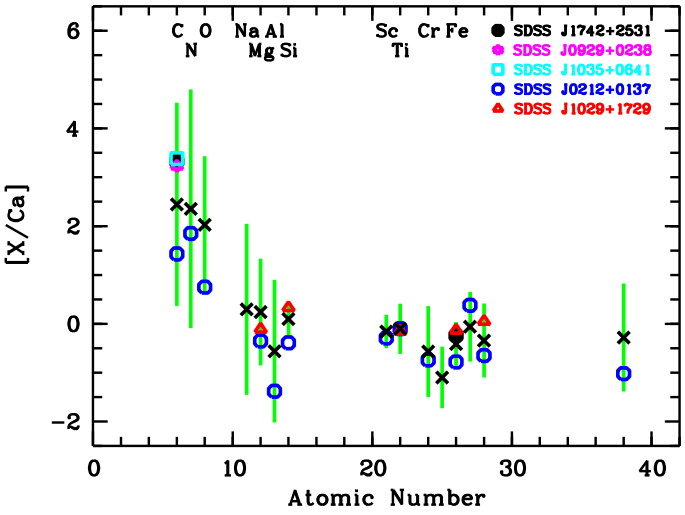

Fig. 7. The ratios of [X/Ca] for elements carbon to yttrium for SDSS J0212+0137 (blue open circle), SDSS J0929+0238 (purple filled circle), SDSS J1035+0641 (cyan open square) and SDSS J1742+2531 (black hexagon). These are compared to the most metal-poor, carbon-normal star SDSS J1029+1729 (Caffau et al. 2012) (red triangles) and to mean [X/Ca] ratios (black ×) in a sample of nine extremely metal-poor CEMP stars: HE 0107-5240 (Christlieb et al. 2004); HE 1327-2326 (Frebel et al. 2008); HE 0557-4840 (Norris et al. 2007); HE 0134-1519, HE 0233-0343, HE 1310-0536 (Hansen et al. 2014); SMSS J0313-6708 (Keller et al. 2014); G 77-61 Plez & Cohen (2005); Plez et al. (2005) and CS 22949-037 (Depagne et al. 2002; Norris et al. 2002). The last star was excluded in the computation of the mean and σ of the elements C and N since it is clearly a "mixed" giant, in the sense specified by Spite et al. (2005). The dispersion around the mean is represented by the bars around the ×, which correspond to 2σ. For all stars we took the abundances of Ca derived from the Ca II lines, except for CS 22949-037 for which we took the Ca I.

5. On the chemical composition and star formation

We next compare the abundances we have determined in the four stars SDSS J0212+0137, SDSS J0929+0238, SDSS J1035+0641, and SDSS J1742+2531 with those observed in other CEMP stars of extremely low metallicity. We selected from the literature the following sample of stars with [Fe/H] < −3.5: HE 0107-5240 (Christlieb et al. 2004); HE 1327-2326 (Frebel et al. 2008); HE 0557-4840 (Norris et al. 2007); HE 0134-1519, HE 0233-0343, HE 1310-0536 (Hansen et al. 2014); SMSS J0313-6708 (Keller et al. 2014); CS 22949-037 (Depagne et al. 2002; Norris et al. 2002); and G 77-61 (Plez & Cohen 2005; Plez et al. 2005). In addition, as an example of a carbon-normal star, we consider the most metal-poor star known to date, SDSS J1029+1729 (Caffau et al. 2012). We note that all six stars known before this paper (see Table A.3) with [Fe/H] < −4.5 (ultra-iron-poor, UIP) are represented in this sample. The only elements that are commonly measured in all of these stars are carbon and calcium, but several other elements are derived in at least two of the stars. Thus, in Fig.7 we plot the [X/Ca] ratios for our program stars. Placing all the measurements for the remaining ten stars in the plot would make it difficult to read. Thus, we plot the individual ratios for SDSS J1029+1729, and for the remaining nine CEMP stars we plot only the mean [X/Ca] value for all elements that have been

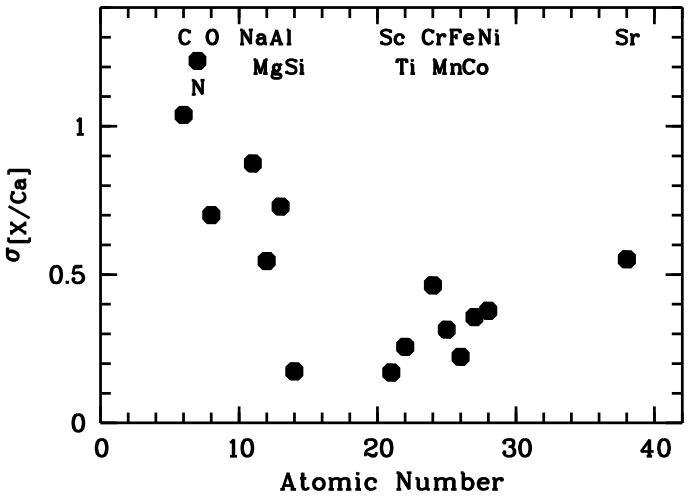

Fig. 8. The σ [X/Ca] for elements that are measured in at least two of the nine CEMP stars (HE 0107-5240 HE 1327-2326, HE 0557-4840, HE 0134-1519, HE 0233-0343, HE 1310-0536, SMSS J0313-6708, CS 22949-037, and G 77-61), as a function of atomic number. As in Fig. 7, C and N in CS 22949-037 were not taken into account.

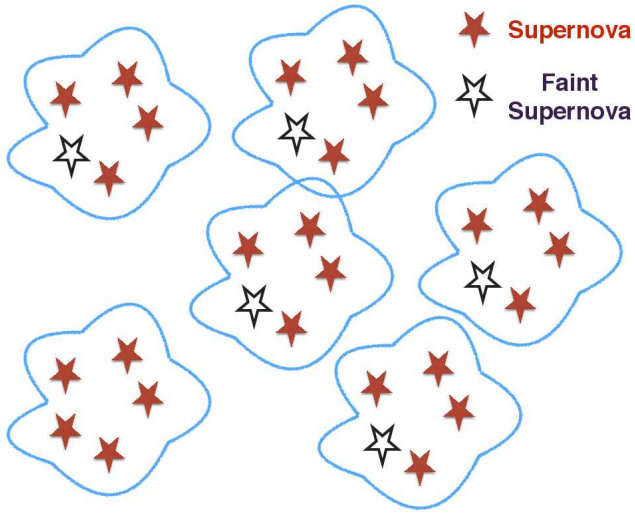

Fig. 9. Scenario discussed in Sect. 5.1. The primordial clouds produce several massive stars, all of which explode as supernovae, but some are "faint" supernovae, with extensive fall-back. The supernova ejecta pollute the cloud determining the chemical composition of the next generation of stars. Occasionally different star formation regions may reciprocally contaminate each other.

measured in at least two of the nine stars. We represent the scatter by drawing 2σ bars around each mean value. Given the differences between the different groups in the treatment of NLTE and granulation effects, we have plotted for all the stars the 1D LTE abundances to make them readily comparable and related all the abundances to the same set of solar abundances. For the Ca abundances we only consider the Ca II abundances for which departures from LTE are negligible (Spite et al. 2012a; Korn et al. 2009; Mashonkina et al. 2007). The exception is CS 22949-037 for which the only LTE Ca abundances available are based on Ca I; we took the LTE value of (Depagne et al. 2002)[7].

5.1. Low scatter in the iron-to-calcium ratio.

We would like to note two features apparent in Fig. 7: *i)* although the present measures have not been used to determine the mean values and dispersions shown in the figure, all the [X/Ca] values are well within the 2σ dispersion, with the only marginal exception of [Si/Ca] in SDSS J0212+0137; and *ii)* the carbon-normal star SDSS J1029+1729 has not been used to determine the mean values and dispersions, but its [X/Ca] values are all within 2σ of the dispersion.

In Fig. 8 we show the dispersion σ in the [X/Ca] ratios for the sample of nine stars detailed above. The plot shows that there is a drop in the dispersion of the [X/Ca] ratios for all the elements heavier than Al, although the stars span 3 dex in A(Fe). The scatter in the [Fe/Ca] ratio is only 0.23 dex. On the contrary, the lighter elements show a much larger scatter, up to 1 dex for carbon. This evidence could be naturally interpreted in terms of a general scenario, already addressed by Limongi, Chieffi & Bonifacio (2003), and Bonifacio et al. (2003), which is based on the fact that the binding energy of a star at the onset of the core collapse increases as the metallicity decreases, the main reason being that these stars are more compact because of the lower opacity and also because of the much lower mass loss they experience during their lifetime. Hence, one expects the number of faint supernovae to increase as the metallicity decreases. In this scenario, the Pop III core collapse supernovae with progenitors lower than $\sim$ 25 $M_\odot$ produced the elemental distribution pattern shown by the normal extremely metal-poor (EMP; for the present discussion this includes all stars with [Fe/H] ≤ -3.0) stars (Limongi & Chieffi 2012). In the clouds already enriched by these supernovae, every now and then a rather massive star exploded with an extended fall-back due to its large binding energy. In this case most of the heavy elements produced in the innermost layers remained locked in the compact remnant and only the lighter elements were mixed in the surrounding. These ejecta were responsible for the variety of abundance patterns shown by the light elements in most of the presently known UIP stars ([Fe/H] < 4.5). The scenario is depicted in Fig. 9.

It is worth noting that the abundance pattern produced by explosive burning does not show a strong dependence on the initial mass of the progenitor, so that even very different initial mass functions (IMFs) would produce a similar abundance pattern: at the extreme, even the ejecta of a single supernova could have been responsible of the observed pattern above Mg (Limongi & Chieffi 2002). No stars at metallicity below –4.5 have yet been detected outside the Galaxy; however, there are now a number of very metal-poor stars (i.e. below –2.5) that are known in Local Group Galaxies, and many are below –3.0. To date, the most metal-poor star known in external galaxies is found in Sculptor and has a metallicity near –4.0 (Tafelmeyer et al. 2010); two more stars of similar metallicity are known in Sculptor (Frebel et al. 2010a; Simon et al. 2015) and six more below –3.0 (Starkenburg et al. 2013; Simon et al. 2015). Other local galaxies with at least one such star are Draco (Shetrone et al. 2001; Fulbright et al. 2004; Cohen & Huang 2009), Sagittarius (Zaggia et al. 2004; Bonifacio et al. 2006; Sbordone et al. 2015, and Monaco et al. in preparation), Fornax (Tafelmeyer et al. 2010), Ursa Minor (Kirby & Cohen 2012; Ural et al. 2015), Sextans (Aoki et al. 2009b; Tafelmeyer et al. 2010), Coma Ber (Frebel et al. 2010b), Ursa Maior II (Frebel et al. 2010b), Segue 1 (Roederer & Kirby 2014; Frebel et al. 2014), Hercules (Koch et al. 2008; Adén et al. 2011), Boo I (Gilmore et al. 2013; Ishigaki et al. 2014b), and

[7] This implies [Fe/Ca] = −0.41; the NLTE value of Spite et al. (2012a) for the Ca I subordinate lines implies [Fe/Ca] = −0.69; the NLTE Ca II of Spite et al. (2012a) implies [Fe/Ca] = −0.88.

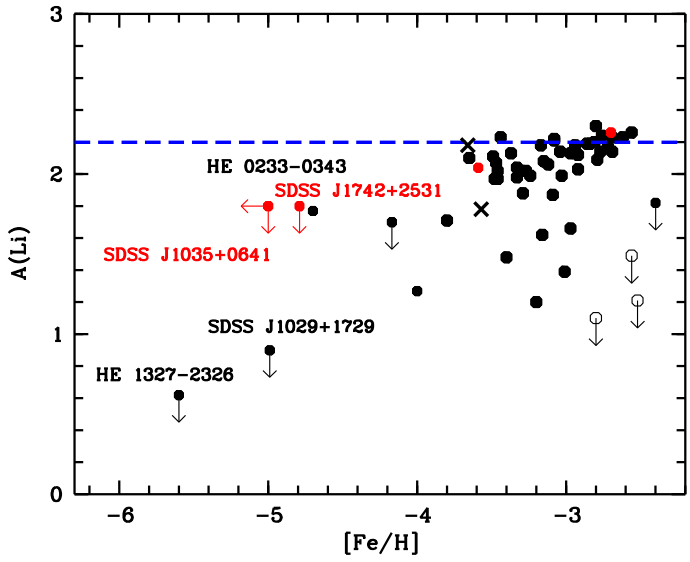

Fig. 10. Lithium abundances, or significant upper limits, in the stars analysed in the present paper (red symbols), compared to those in other extremely metal-poor unevolved stars (Frebel et al. 2008; Sbordone et al. 2010; Bonifacio et al. 2012; Caffau et al. 2012; Hansen et al. 2014) (black symbols). The two components of the binary system CS 22876-32 (González Hernández et al. 2008) are shown as crosses. The upper limits shown as open symbols are G 186-26, G 122-69, and G 139-8 from Norris et al. (1997a). The blue dashed line is the level of the Spite plateau as determined by Sbordone et al. (2010).

Boo II (Koch & Rich 2014). Particularly relevant to the present discussion is the discovery of a CEMP-no star in the Sculptor dwarf spheroidal (Skúladóttir et al. 2015). The conclusion of the authors is that the fraction of CEMP-no stars in Sculptor seems to be significantly lower than in the Galactic Halo. In our scenario this could be explained either with a lower frequency of faint SNe in Sculptor, or with shallower potential wells that can allow the formation of the second generation of stars. Another CEMP-no star of extremely low metallicity was previously discovered in Bootes I (Lai et al. 2011; Gilmore et al. 2013) and this one also lies in the *low-carbon band*. In any case the presence of at least two CEMP-no stars outside our Galaxy prompts us to search for a formation mechanism that is universal. Clearly, further scrutiny of the EMP populations in Local Group galaxies, as can be afforded by multi-object spectrographs on 30 m class telescopes (Evans et al. 2015), is of the highest interest.

We also note that the upper limit for the [Fe/Ca] ratio in SMSS J0313-6708 is consistent with the values observed in the other stars. If the iron abundance in this star were measured to be up to 0.4 dex below the current upper limit it would be similar to the others; only if it were much lower would it be definitely peculiar. If our scenario is correct the ratios of all elements heavier than Si to Ca in SMSS J0313-6708 ought to be within the mean trends shown in Figs. 7 and 8, although its [C/Ca] and [Mg/Ca] ratios are at several σ from the mean.

5.2. Lithium

There are now five known unevolved stars with iron abundance below −4.5: HE 1327-2326 (Frebel et al. 2005), SDSS J1029+1729 (Caffau et al. 2012), HE 0233-0343 (Hansen et al. 2014), SDSS J1742+2531 (Caffau et al. 2013a and this paper) and SDSS J1035+0641 (this paper). SDSS J1742+2531 and SDSS J1035+0641 have no measurable lithium, like HE 1327-2326 and SDSS J1029+1729, at variance with most of the stars found at higher iron abundance with similar atmospheric parameters. The situation is shown in Fig. 10. HE 0233-0343 is very similar to SDSS J1742+2531 both for atmospheric parameters and chemical abundances of C, Ca, and Fe, but it has a detectable lithium doublet that implies A(Li)=1.77 (Hansen et al. 2014), thus roughly a factor of three below the Spite plateau.

The Spite plateau meltdown, highlighted by Aoki et al. (2009a) and Sbordone et al. (2010), is the large number of stars at metallicity below −3.0 solar, which have lithium abundances lower than the Spite plateau, but still measurable (see figure 3 in Spite et al. 2012b). In three of the above-mentioned UIP stars the lithium abundance could not be measured, and it is intriguing to consider the possibility that the atmospheres of these stars are indeed totally devoid of lithium. How did this happen? Is this related to the very low iron abundance of these stars? We note that owing to the difference in the C abundances, their total metallicity Z is indeed very different.

The observation of HE 0233-0343 implies that the phenomenon responsible for the total destruction of lithium is not effective in all cases. It is, however, natural to suppose that it is the same phenomenon that is responsible for the lithium depletion in HE 0233-0343 and for the Spite plateau meltdown.

A possible explanation is that all these stars were born with high rotational velocities as a consequence of the role of fragmentation in their formation, as argued in section 5.3 and as supported by the simulations of Stacy et al. (2011a, 2013). We note that the gas out of which the first stars form was likely to be strongly magnetised. Any pre-existing magnetic field was amplified to dynamically significant levels by the small-scale turbulent dynamo which converts parts of the kinetic energy associated with the accretion flow in the star-forming parts of the halo into magnetic energy (Schleicher et al. 2010; Sur et al. 2010; Schober et al. 2012). In principle, magnetic fields can remove angular momentum from the system by magnetic braking (e.g. Mouschovias 1985; Hennebelle & Ciardi 2009). However, the efficiency of this process is strongly reduced in turbulent fields with a highly tangled morphology (Seifried et al. 2012, 2013), and so an appreciable fraction of the angular momentum is thought to remain in the system. This –together with the fact that primordial stars are expected to have very weak winds (Ekström et al. 2008)– supports the hypothesis that these stars remain fast rotators at least during all of their pre-MS and a good part of their MS phase (Maeder & Meynet 2012). Rotational mixing would then bring the material below the region of Li-burning, leading to the total destruction of Li in these stars. As the metal content increases the star formation mode shifts to a more standard Pop II formation mode, with lower rotational velocities and less Li destruction. In this scenario the Spite plateau meltdown would simply mark the transition between the Pop III and Pop II star formation mode.

A second, related, scenario has been proposed by Molaro et al. (2012). They assume Li is significantly destroyed in the pre-MS phase by overshoot mixing, and then partially restored by late accretion of fresh non-Li depleted material. The extreme objects, such as SDSS J1742+2531, SDSS J1029+1729, SDSS J1035+0641 and HE 1327-2326, simply lacked the late accretion phase because they formed by fragmentation, and as a result the proto-star was ejected from the gas reservoir.

Finally, we wish to propose a third possible scenario that does not invoke high rotation in the early stages of the star's life. The first stars formed in dark-matter minihaloes (see Bromm 2013, and references therein). The concept of minihaloes that

eventually merge to form a galaxy is at the heart of the cold dark matter, with Cosmological constant (Λ-CDM) scenario of hierarchical galaxy formation. If all the first-generation stars explode as SNe, with typical energies of 10^{51} ergs, then the remaining gas in the minihalo is blown out and no further star formation can take place. However, in some minihaloes a few typical SNe explode in addition to faint SNe. In this case the gas is not blown out and a second generation of stars may form. The second-generation stars may have both a CEMP-no chemical composition or a normal EMP composition, depending on the mass of the ejecta contributed by faint and normal SNe. However, in all these stars the Li content would be lower than that present in the primordial gas. The SNe ejecta being Li-free, the resulting Li abundance would simply depend on the amount of dilution of the SN ejecta with pristine material. If we assume that many of the stars with [Fe/H]$\lesssim -2.8$ have been formed in such minihaloes, this could explain the Spite plateau meltdown. In this case the most metal-poor stars would simply be an extreme case of stars formed from ejecta very little diluted with pristine material. Once the galaxy is assembled, through the merging of many minihaloes, a standard chemical evolution, with well-mixed matter begins (Prantzos 2012). The final result is that all the Li-free material of the SNe ejecta dilutes the primordial lithium abundance. This could solve the cosmological Li problem.

In all three of the above scenarios the case of HE 0233-0343 could be accommodated if we assume that the phenomenon has various degrees of efficiency. In the case of rotationally induced mixing, this should be partially inhibited by some kind of braking (magnetic or other). In the case of late accretion, this should be allowed to proceed long enough to restore the lithium to the observed abundance. In the case of mixing of primordial matter with SNe ejecta in minihaloes, it is the mass ratio of the two materials that governs the final Li abundance.

5.3. Implications on the formation of low-mass stars in metal-poor gas

Star formation in metal-free or extremely metal-poor environments is more complex than previously thought. While early simulations of the formation of primordial stars suggested masses above 100 $M_\odot$ (Omukai & Palla 2001, 2003; Abel et al. 2002; Bromm et al. 2002), more recent work in early star formation acknowledges the importance of turbulence (Clark et al. 2011a; Greif et al. 2011a,b), variations of halo properties (Hosokawa et al. 2012; Hirano et al. 2014), cosmological streaming velocities (Tseliakhovich & Hirata 2010; Greif et al. 2011a; Maio et al. 2011; Stacy et al. 2011b; Tseliakhovich et al. 2011), and even magnetic fields (Schleicher et al. 2008; Peters et al. 2014) or potentially dark-matter annihilation (Iocco 2008; Spolyar et al. 2009; Smith et al. 2012). All these processes influence the fragmentation properties of the star forming gas and consequently modify the resulting stellar mass spectrum. As discussed in Section 4.1, current studies predict a wide range of masses all the way down into the substellar regime. However, a full consensus on the IMF of primordial as well as of extremely metal-poor stars has yet to emerge, and so further investigations are required. As soon as the metallicity rises above a certain threshold, which is thought to lie between 10^{-6} and 10^{-5} $Z_\odot$ (e.g. Omukai et al. 2005; Schneider et al. 2012a; Glover 2013), two main cooling channels emerge which could lead to the efficient formation of low-mass stars and result in a stellar mass spectrum similar to the present-day IMF (Kroupa 2002; Chabrier 2003). These cooling processes are

- fine structure transitions of C II and O I (Bromm & Loeb 2003) and
- dust cooling (Schneider et al. 2006; Omukai et al. 2008; Dopcke et al. 2011; Schneider et al. 2012a; Dopcke et al. 2013).

SDSS J1742+2531 is the seventh star discovered with [Fe/H] < -4.5 and out of seven, six are CEMP stars (on the *low-carbon band*) and only one, SDSS J1029+1729, is a carbon-normal star.

The *low-carbon band* places all these CEMP stars in the "permitted zone" of the Bromm & Loeb (2003) theory, thus making formation via metal-line cooling viable. This is not the case for SDSS J1029+1729, for which dust cooling appears necessary (Schneider et al. 2012b; Klessen et al. 2012; Chiaki et al. 2014).

It would be tempting to conclude, as Norris et al. (2013) and Gilmore et al. (2013) did, that the CEMP stars of the *low-carbon band* were formed via line cooling, while SDSS J1029+1729 formed via dust cooling. However, even for the C-enhanced gas, line cooling only lowers the Jeans masses (and as a consequence stellar masses) to values largely in excess of 10 $M_\odot$. Clearly, in order to form the low-mass objects observed, one would need to resort to a high-density cooling process, such as dust cooling. This is the only process that brings the gas into the right regime of masses consistent with the observations (Omukai et al. 2005; Clark et al. 2008; Klessen et al. 2012; Schneider et al. 2012a,b; Dopcke et al. 2013; Chiaki et al. 2014, 2015). It seems thus more realistic to assume that all the stars in Fig. 7 were formed by dust cooling, irrespective of their carbon content.

We note, however, that the above arguments are based solely on thermodynamics. If we also consider the dynamics of the collapsing cloud it turns out that even completely metal-free gas can make low-mass objects simply by disc fragmentation (e.g. Clark et al. 2011a; Greif et al. 2011b, 2012) because the gas is almost isothermal over a wide range of densities[8]. The mass load onto the accretion disc exceeds its ability to transport material inwards, and it fragments. This fragmentation is not as widespread as with dust cooling. The expected IMF is flat (Dopcke et al. 2013), which means that it is still top-heavy with respect to today's standards, but it is possible to make low-mass objects in the mass range of the stars in Fig. 7. Therefore, in principle, all these stars may have been formed without resorting to either dust or metal-line cooling.

In a recent paper, Cooke & Madau (2014) proposed a numerical model of the chemical enrichment produced by the first generation of stars, and looked at the resulting chemical composition irrespective of the mechanism needed to form the next generation of low-mass stars. Their model has several points in common with our proposed scenario. In particular, they assume that the first stellar generations are formed in minihaloes of a mass of a few millions of solar masses. In these haloes one or several massive stars are formed. Cooke & Madau (2014) recognise the important link between the explosion energy of the resulting supernovae and the ability of the minihalo to retain gas and thus form a new generation of stars. The consequence is that the minihaloes that host faint (low energy) SNe are those that are more likely to form second-generation stars, and because of the presence of the faint SNe these are indeed C-enhanced. This model reproduces well the increase in the fraction of CEMP stars at low metallicity and the role of faint SNe is very similar to the scenario that we propose. However, the model is less successful in reproducing the detailed abundances of the EMP stars. In

[8] The equation of state can be expressed as $P \propto \rho^\gamma$ with $1.05 \lesssim \gamma \lesssim 1.1$ and ρ density, with no explicit dependence on temperature.

particular at the lowest metallicities all the stars seem to lie at [C/Fe] values much higher than those preferred by the models. Here we have presented data for four more such stars, suggesting that these high [C/Fe] values, which correspond simply to the *low-carbon band* discussed here, are the norm at low metallicities and not the exception. This rules out exotic explanations like enrichment from AGB stars or CNO boosted nucleosynthesis (see Cooke & Madau 2014, and references therein). We believe that the most likely possibility is the one proposed by Cooke & Madau (2014), that the mixing of the SNe ejecta is not uniform. In Sect. 4.2 we suggest that the existence of the *low-carbon band* provides a strong constraint to the minimum dilution of SNe ejecta necessary for star formation. In the context of the Cooke & Madau (2014) models we argue that the width of the band should provide a constraint on the dispersion in dilutions encountered. It would be interesting to run models of the type of the Cooke & Madau (2014) models, with a variable dilution to see if it is possible to reproduce the *low-carbon band*.

5.4. Alternative scenarios

There are, of course, alternative scenarios to our preferred faint supernovae scenario that may explain the occurrence of CEMP stars of extremely low metallicity. We refer the reader to the introduction of the recent paper by Maeder et al. (2014) who list as many as five possible scenarios and to the extensive review of Karlsson et al. (2013) on the chemical signatures of the first stars. Here we wish only to mention the one that we believe is the most serious competitor to the faint supernova scenario: rapidly rotating massive stars. A rapidly rotating massive star may, during its main sequence lifetime, bring C and N to the surface. Plez et al. (2005) invoked this mechanism to explain the large N abundance and low $^{12}C/^{13}C$ ratio in one of the first CEMP stars of extremely low metallicity discovered: G 77-61. The role of rapidly rotating massive stars in producing CEMP stars has often been discussed in the literature (Meynet et al. 2006; Chiappini et al. 2006; Hirschi 2007; Meynet et al. 2010; Maeder et al. 2014). In the presence of rapid rotation, N in particular would be greatly increased by rotation during the central He burning phase when a tail of C produced by the He burning is transported to the base of the H burning shell by rotationally induced mixing, and then rapidly converted into N by the CNO cycle. In particular, we expect that a generation of stars rotating initially at 300 km/s, integrated over a Salpeter IMF, would produce ejecta (but not necessarily wind) with a C/N ratio of the order of 17 (Limongi and Chieffi in preparation), while the analogous generation of non-rotating stars would provide a C/N ratio of the order of 3500. The same holds for the $^{12}C/^{13}C$ ratio that turns from 350000 to 2000 from v=0 to v=300. It is worth noting that rotation should not be extreme, in the sense that it must not lead to a full mixing of the star because some active H burning must be still present when C is produced by the central He burning.

In the future we plan to make a detailed comparison of the predictions of faint supernovae and rapidly rotating massive stars.

6. Conclusions

We have determined the iron abundance in SDSS J1742+2531 to be [Fe/H] = −4.8. This increases the sample of known stars with [Fe/H] < −4.5 to seven. We could not measure the iron abundance in SDSS J1035+0641, yet our 3σ upper limit of −5.00 classifies it as the eighth such star, supported also by its extremely low Ca abundance ([Ca/H] = −5.0). Both stars are carbon enhanced (CEMP), thus the sample of the eight most iron-poor stars is composed of seven CEMP stars and one carbon-normal star (SDSS J1029+1729).

Based on the measured [X/Ca] ratios in a sample of CEMP stars, and theoretical predictions of nucleosynthesis in zero-metallicity supernovae, we have proposed a scenario in which the metals observed in these stars were produced by a few zero-metallicity SNe. The carbon abundances of the program stars confirm the bimodal distribution in CEMP stars, with the CEMP-no stars occupying a *low-carbon band* identified by Spite et al. (2013). We have proposed an interpretation of this bimodality: the stars on the *high-carbon band*, all of which are binaries (Starkenburg et al. 2014), are the result of mass-transfer from an AGB star in a binary system, while the *low-carbon band* stars reflect the abundances of the gas out of which they were formed, the high-carbon abundance is the result of the ejecta of a faint supernova.

This scenario is also supported by the theoretical predictions that the zero-metallicity stars are not formed in isolation but are formed in groups, and possibly as multiple stars (Clark et al. 2008; Stacy et al. 2010; Clark et al. 2011a,b; Greif et al. 2011b, 2012; Stacy & Bromm 2013). The idea that several massive Pop III stars may pollute a primordial cloud, and that subsequently low-mass stars can form in the high-density shocks was already proposed by Cayrel (1986). However, at that time no stars as metal-poor as those discussed here were known, and it was suggested that this mechanism could enrich the gas up to one hundredth of the solar value or even above. Our proposed scenario, following the ideas of Bonifacio et al. (2003) and Limongi, Chieffi & Bonifacio (2003), requires a few SNe of mass less than $\sim 25 M_{\odot}$. Since our scenario requires more than one SNe, it departs significantly from other attempts to explain the abundance pattern of these stars by the ejecta of a single exotic SN (see e.g. Umeda & Nomoto 2003; Iwamoto et al. 2005; Izutani et al. 2009; Joggerst et al. 2010; Ishigaki et al. 2014a, and references therein). Our scenario explains well the low star-to-star scatter in the [X/Ca] ratios (a factor of two, at most) for elements heavier than Mg, in spite of the large span in [Fe/H] displayed by these stars. The large scatter in the [X/Ca] ratios for the lighter elements, and in particular the CEMP nature of some of the stars, are determined by the presence, among the SNe that produced the metals, of at least one faint SN. The fact that seven out of eight stars found to have [Fe/H] below –4.5 are CEMP, suggests that the occurrence of the faint SNe is a rather common event probably because the binding energy of the lower metallicity stars at the onset of the core collapse is larger, thus favouring fall-back, and the faintness of the SN. The statistics are clearly scanty and before drawing conclusions on the frequency of faint SNe one should study possible selection biases. This is not trivial given that the seven most iron-poor stars have been selected from three different surveys (Hamburg ESO, SDSS, and SMSS) with different follow-up procedures. The fact that three of the eight stars have been selected by our group from SDSS using the same criteria and include one carbon-normal (SDSS J1029+1729) and two CEMP (SDSS J1035+0641 and SDSS J1742+2531) suggests that there is no strong bias in favour of or against the selection of CEMP stars.

Very interestingly, SDSS J1742+2531 and SDSS J1035+0641 do not show any detectable lithium, and this characteristic is shared by two of the other unevolved stars of the sample (SDSS J1029+1729 and HE 1327-2326). We proposed three possible scenarios to explain these Li-poor stars. In two of the scenarios they were formed by fragmentation and this resulted in the destruction of lithium in the pre-main-

sequence phase, either through rotational mixing or owing to the lack of the late accretion phase as proposed by Molaro et al. (2012). A third scenario requires that these stars were formed within a minihalo, in which the Li-free SN ejecta were mixed with primordial gas. Their formation must have taken place before the minihaloes merged to form the Galaxy. In all three cases these stars had a different formation with respect to the stars with higher [Fe/H]. The case of HE 0233-0343, which is very similar to SDSS J1742+2531 except for the lithium abundance, implies that even in this star formation mode some lithium can survive. It is, however, remarkable that the lithium observed in this star is still almost a factor of three below the Spite plateau, and similar to the value observed in many of the stars of the Spite plateau meltdown.

Among the different mechanisms for the formation of these UIP stars, the Bromm & Loeb (2003) cooling mechanism is viable for all the CEMP stars, yet it still requires either a fragmentation of the gas cloud at the late stages of the collapse or an additional high-density cooling mechanism. On the other hand, all forms of dust cooling (Schneider et al. 2006; Omukai et al. 2008; Dopcke et al. 2011; Schneider et al. 2012a; Dopcke et al. 2013) are viable for all the UIP stars, CEMP or not. Disc fragmentation (Clark et al. 2011a; Greif et al. 2011b, 2012), is also a possible formation mechanism for all these stars, and it would also allow the formation of primordial low-mass stars.

The indirect evidence coming from the lack of lithium in three of the four unevolved stars, suggests a prominent role of disc fragmentation, either in the presence of dust or not. A direct confirmation of this mechanism would be the detection of a low-mass star totally devoid of metals. The search of such stars must continue, and an interesting prospect is offered by an all-sky, unbiased survey such as Gaia[9].

Acknowledgements. The project was funded by FONDATION MERAC. PB, EC, PF, MS, FS, and RC acknowledge support from the Programme National de Cosmologie et Galaxies (PNCG) and Programme National de Physique Stellaire of the Institut National de Sciences de l'Univers of CNRS. EC, RKS, HGL, NC, SCOG, and LS acknowledge financial support by the Sonderforschungsbereich SFB881 "The Milky Way System" (subprojects A4, A5, B1, B2 and B8) of the German Research Foundation (DFG). ML and AC acknowledge financial support from PRIN MIUR 2010-2011, project "The Chemical and dynamical Evolution of the Milky Way and Local Group Galaxies", prot. 2010LY5N2T. RSK furthermore acknowledges support from the European Research Council under the European Community's Seventh Framework Programme (FP7/2007-2013) via the ERC Advanced Grant STARLIGHT (project number 339177). LS acknowledges the support of Project IC120009 "Millennium Institute of Astrophysics (MAS)" of Iniciativa Científica Milenio del Ministerio de Economía, Fomento y Turismo de Chile EC and PM acknowledge support from the international team #272 lead by C. M. Coppola EUROPA- Early Universe: Research On Plasma Astrochemistry" at ISSI (International Space Science Institute) in Bern.

References

Abazajian, K. N., Adelman-McCarthy, J. K., Agüeros, M. A., et al. 2009, ApJS, 182, 543
Abel, T., Bryan, G. L., & Norman, M. L. 2002, Science, 295, 93
Adén, D., Eriksson, K., Feltzing, S., et al. 2011, A&A, 525, A153
Ahn, C. P., Alexandroff, R., Allende Prieto, C., et al. 2012, ApJS, 203, 21
Aihara, H., Allende Prieto, C., An, D., et al. 2011a, ApJS, 193, 29
Aihara, H., Allende Prieto, C., An, D., et al. 2011b, ApJS, 195, 26
Alvarez R., Plez B., 1998, A&A 330, 1109
Andrievsky, S. M., Spite, M., Korotin, S. A., et al. 2007, A&A, 464, 1081
Aoki, W., Frebel, A., Christlieb, N., et al. 2006, ApJ, 639, 897
Aoki, W., Beers, T. C., Christlieb, N., et al. 2007, ApJ, 655, 492
Aoki, W., Beers, T. C., Sivarani, T., et al. 2008, ApJ, 678, 1351
Aoki, W., Barklem, P. S., Beers, T. C., et al. 2009a, ApJ, 698, 1803
Aoki, W., Arimoto, N., Sadakane, K., et al. 2009b, A&A, 502, 569
Aoki, W., Beers, T. C., Lee, Y. S., et al. 2013, AJ, 145, 13

[9] http://sci.esa.int/gaia/

Aoki, W., Suda, T., Beers, T. C., & Honda, S. 2015, AJ, 149, 39
Ballester, P., Modigliani, A., Boitquin, O., et al. 2000, The Messenger, 101, 31
Beers, T. C., & Christlieb, N. 2005, ARA&A, 43, 531
Behara, N. T., Bonifacio, P., Ludwig, H.-G., et al. 2010, A&A, 513, A72
Bisterzo, S., Gallino, R., Straniero, O., Cristallo, S., Käppeler, F. 2010, MNRAS, 404, 1529
Bisterzo, S., Gallino, R., Straniero, O., Cristallo, S., Käppeler, F. 2011, MNRAS, 418, 284
Bonifacio, P., Molaro, P., Beers, T. C., & Vladilo, G. 1998, A&A, 332, 672
Bonifacio, P., Limongi, M., & Chieffi, A. 2003, Nature, 422, 834
Bonifacio, P., Zaggia, S., Sbordone, L., et al. 2006, in "Chemical Abundances and Mixing in Stars in the Milky Way and its Satellites" ESO ASTROPHYSICS SYMPOSIA, S. Randich & L. Pasquini eds., p. 232
Bonifacio, P., Spite, M., Cayrel, R., et al. 2009, A&A, 501, 519
Bonifacio, P., Sbordone, L., Caffau, E., et al. 2012, A&A, 542, A87
Bonifacio, P., Caffau, E., Ludwig, H.-G., et al. 2013, Memorie della Societa Astronomica Italiana Supplementi, 24, 138
Bromm, V. 2013, Reports on Progress in Physics, 76, 112901
Bromm, V., & Loeb, A. 2003, Nature, 425, 812
Bromm, V., Coppi, P. S., & Larson, R. B. 2002, ApJ, 564, 23
Caffau, E., Ludwig, H.-G., Steffen, M., Freytag, B., & Bonifacio, P. 2011a, Sol. Phys., 268, 255
Caffau, E., Bonifacio, P., François, P., et al. 2012, A&A, 542, A51
Caffau, E. et al. 2013a A&A, 560, A15
Caffau, E. et al. 2013b, A&A, 560, A71
Carollo, D., Beers, T. C., Bovy, J., et al. 2012, ApJ, 744, 195
Carollo, D., Freeman, K., Beers, T. C., et al. 2014, ApJ, 788, 180
Carswell, R. F., Becker, G. D., Jorgenson, R. A., Murphy, M. T., & Wolfe, A. M. 2012, MNRAS, 422, 1700
Cassisi, S., Castellani, M., Caputo, F., & Castellani, V. 2004, A&A, 426, 641
Castelli, F. & Kurucz, R. L. 2003, in IAU Symposium 210, ed. N. Piskunov, W. W. Weiss, & D. F. Gray, A20, arXiv:astro-ph/0405087v1
Cayrel, R. 1986, A&A, 168, 81
Cayrel, R. 1988, IAU Symp. 132: The Impact of Very High S/N Spectroscopy on Stellar Physics, 132, 345
Chabrier, G. 2003, PASP, 115, 763
Chiaki, G., Schneider, R., Nozawa, T., et al. 2014, MNRAS, 439, 3121
Chiaki, G., Marassi, S., Nozawa, T., et al. 2015, MNRAS, 446, 2659
Chiappini, C., Hirschi, R., Meynet, G., et al. 2006, A&A, 449, L27
Christlieb, N., Gustafsson, B., Korn, A. J., et al. 2004, ApJ, 603, 708
Clark, P. C., Glover, S. C. O., & Klessen, R. S. 2008, ApJ, 672, 757
Clark, P. C., Glover, S. C. O., Smith, R. J., et al. 2011a, Science, 331, 1040
Clark, P. C., Glover, S. C. O., Klessen, R. S., & Bromm, V. 2011b, ApJ, 727, 110
Cohen, J. G., & Huang, W. 2009, ApJ, 701, 1053
Cohen, J. G., Christlieb, N., Thompson, I., et al. 2013, ApJ, 778, 56
Cooke, R. J., & Madau, P. 2014, ApJ, 791, 116
Cooke, R., Pettini, M., Steidel, C. C., Rudie, G. C., & Jorgenson, R. A. 2011, MNRAS, 412, 1047
Cooke, R., Pettini, M., & Murphy, M. T. 2012, MNRAS, 425, 347
Dawson, K. S., Schlegel, D. J., Ahn, C. P., et al. 2013, AJ, 145, 10
Depagne, E., Hill, V., Spite, M., et al. 2002, A&A, 390, 187
Dopcke, G., Glover, S. C. O., Clark, P. C., & Klessen, R. S. 2011, ApJ, 729, L3
Dopcke, G., Glover, S. C. O., Clark, P. C., & Klessen, R. S. 2013, ApJ, 766, 103
Dutta, R., Srianand, R., Rahmani, H., et al. 2014, MNRAS, 440, 307
Ekström, S., Meynet, G., Chiappini, C., Hirschi, R., & Maeder, A. 2008, A&A, 489, 685
Evans, C., Puech, M., Afonso, J., et al. 2015, arXiv:1501.04726
François, P., Depagne, E., Hill, V., et al. 2007, A&A, 476, 935
Frebel, A., Aoki, W., Christlieb, N., et al. 2005, Nature, 434, 871
Frebel, A., Christlieb, N., Norris, J. E., et al. 2006, ApJ, 652, 1585
Frebel, A., Collet, R., Eriksson, K., Christlieb, N., & Aoki, W. 2008, ApJ, 684, 588
Frebel, A., Kirby, E. N., & Simon, J. D. 2010a, Nature, 464, 72
Frebel, A., Simon, J. D., Geha, M., & Willman, B. 2010b, ApJ, 708, 560
Frebel, A., Simon, J. D., & Kirby, E. N. 2014, ApJ, 786, 74
Fulbright, J. P., Rich, R. M., & Castro, S. 2004, ApJ, 612, 447
Fumagalli, M., O'Meara, J. M., & Prochaska, J. X. 2011, Science, 334, 1245
Gilmore, G., Norris, J. E., Monaco, L., et al. 2013, ApJ, 763, 61
Glover, S. 2013, Astrophysics and Space Science Library, 396, 103
González Hernández, J. I., Bonifacio, P., Ludwig, H.-G., et al. 2008, A&A, 480, 233
Gratton, R. G., Carretta, E., Eriksson, K., & Gustafsson, B. 1999, A&A, 350, 955
Greif, T. H., 2014, Computational Astrophysics and Cosmology, submitted; arXiv:1410.3482
Greif, T. H., White, S. D. M., Klessen, R. S., & Springel, V. 2011a, ApJ, 736, 147
Greif, T. H., Springel, V., White, S. D. M., et al. 2011b, ApJ, 737, 75
Greif, T. H., Bromm, V., Clark, P. C., et al. 2012, MNRAS, 424, 399

Gustafsson, B., Edvardsson, B., Eriksson, K., Graae-Jørgensen, U., Nordlund, Å., & Plez, B. 2008, A&A 486, 951
Hansen, C. J., Nordström, B., Bonifacio, P., et al. 2011, A&A, 527, A65
Hansen, T., Hansen, C. J., Christlieb, N., et al. 2014, ApJ, 787, 162
Hennebelle, P., & Ciardi, A. 2009, A&A, 506, L29
Hill, V., Plez, B., Cayrel, R., et al. 2002, A&A, 387, 560
Hirano, S., Hosokawa, T., Yoshida, N., et al. 2014, ApJ, 781, 60
Hirschi, R. 2007, A&A, 461, 571
Hosokawa, T., Yoshida, N., Omukai, K., & Yorke, H. W. 2012, ApJ, 760, LL37
Iocco, F. 2008, ApJ, 677, L1
Ishigaki, M. N., Tominaga, N., Kobayashi, C., & Nomoto, K. 2014a, ApJ, 792, L32
Ishigaki, M. N., Aoki, W., Arimoto, N., & Okamoto, S. 2014b, A&A, 562, AA146
Iwamoto, N., Umeda, H., Tominaga, N., Nomoto, K., & Maeda, K. 2005, Science, 309, 451
Izutani, N., Umeda, H., & Tominaga, N. 2009, ApJ, 692, 1517
Jester, S., Schneider, D. P., Richards, G. T., et al. 2005, AJ, 130, 873
Joggerst, C. C., Almgren, A., Bell, J., et al. 2010, ApJ, 709, 11
Karlsson, T., Bromm, V., & Bland-Hawthorn, J. 2013, Reviews of Modern Physics, 85, 809
Keller, S. C., Bessell, M. S., Frebel, A., et al. 2014, Nature, 506, 463
Kirby, E. N., & Cohen, J. G. 2012, AJ, 144, 168
Klessen, R. S., Glover, S. C. O., & Clark, P. C. 2012, MNRAS, 421, 3217
Kobayashi, C., Ishigaki, M. N., Tominaga, N., & Nomoto, K. 2014, ApJ, 785, L5
Koch, A., McWilliam, A., Grebel, E. K., Zucker, D. B., & Belokurov, V. 2008, ApJ, 688, L13
Koch, A., & Rich, R. M. 2014, ApJ, 794, 89
Korn, A. J., Shi, J., & Gehren, T. 2003, A&A, 407, 691
Korn, A. J., Richard, O., Mashonkina, L., et al. 2009, ApJ, 698, 410
Kroupa, P. 2002, Science, 295, 82
Kulkarni, G., Rollinde, E., Hennawi, J. F., & Vangioni, E. 2013, ApJ, 772, 93
Lai, D. K., Lee, Y. S., Bolte, M., et al. 2011, ApJ, 738, 51
Lee, Y. S., Beers, T. C., Masseron, T., et al. 2013, AJ, 146, 132
Li, H.-N., Zhao, G., Christlieb, N., et al. 2015, ApJ, 798, 110
Limongi, M., & Chieffi, A. 2002, PASA, 19, 246
Limongi, M., Chieffi, A., Bonifacio, P. 2003, ApJ, 594, L123
Limongi, M., Chieffi, A. 2012, ApJS, 199, 38
Lodders, K., Plame, H., & Gail, H.-P. 2009, Landolt-Börnstein - Group VI Astronomy and Astrophysics Numerical Data and Functional Relationships in Science and Technology Volume 4B: Solar System. Edited by J.E. Trümper, 2009, 4.4., 44
Lucatello, S., Tsangarides, S., Beers, T. C., et al. 2005, ApJ, 625, 825
Ludwig, H.-G., Bonifacio, P., Caffau, E., et al. 2008, Physica Scripta Volume T, 133, 014037
Maeder, A., & Meynet, G. 2012, Reviews of Modern Physics, 84, 25
Maeder, A., Meynet, G., & Chiappini, C. 2014, arXiv:1412.5754
Maio, U., Koopmans, L. V. E., & Ciardi, B. 2011, MNRAS, 412, L40
Mashonkina, L., Korn, A. J., & Przybilla, N. 2007, A&A, 461, 261
Mashonkina, L., Ludwig, H.-G., Korn, A., Sitnova, T., & Caffau, E. 2013, MSAIS, 24, 120
Masseron, T., Johnson, J. A., Plez, B., et al. 2010, A&A, 509, A93
Masseron, T., Johnson, J. A., Lucatello, S., et al. 2012, ApJ, 751, 14
Meynet, G., Ekström, S., & Maeder, A. 2006, A&A, 447, 623
Meynet, G., Hirschi, R., Ekstrom, S., et al. 2010, A&A, 521, AA30
Molaro, P., Centurión, M., D'Odorico, V., & Péroux, C. 2004, Origin and Evolution of the Elements, 39
Molaro, P. 2006, ESO/Arcetri Workshop on "Chemical Abundances and Mixing in Stars in the Milky Way and its Satellites", eds., L. Pasquini and S. Randich (Springer-Verlag Series, "ESO Astrophysics Symposia") p. 256
Molaro, P., Bressan, A., Barbieri, M., Marigo, P., & Zaggia, S. 2012, Memorie della Societa Astronomica Italiana Supplementi, 22, 233
Mouschovias, T. C. 1985, A&A, 142, 41
Norris, J. E., Ryan, S. G., Beers, T. C., & Deliyannis, C. P. 1997a, ApJ, 485, 370
Norris J. E., Ryan S. G., & Beers T. C. 1997b, ApJ, 488, 350
Norris, J. E., Ryan, S. G., Beers, T. C., Aoki, W., & Ando, H. 2002, ApJ, 569, L107
Norris, J. E., Christlieb, N., Korn, A. J., Eriksson, K., Bessell, M. S., Beers, T. C., Wisotzki, L., & Reimers, D. 2007, ApJ, 670, 774
Norris, J. E., Yong, D., Bessell, M. S., et al. 2013, ApJ, 762, 28
Omukai, K., & Palla, F. 2001, ApJ, 561, L55
Omukai, K., & Palla, F. 2003, ApJ, 589, 677
Omukai, K., Tsuribe, T., Schneider, R., & Ferrara, A. 2005, ApJ, 626, 627
Omukai, K., Schneider, R., & Haiman, Z. 2008, ApJ, 686, 801
Peters, T., Schleicher, D. R. G., Smith, R. J., Schmidt, W., & Klessen, R. S. 2014, MNRAS, 442, 3112
Placco, V. M., Kennedy, C. R., Beers, T. C., et al. 2011, AJ, 142, 188
Plez, B. 2012, Turbospectrum: Code for spectral synthesis, astrophysics Source Code Library
Plez, B., & Cohen, J. G. 2005, A&A, 434, 1117
Plez, B., Cohen, J. G., & Meléndez, J. 2005, From Lithium to Uranium: Elemental Tracers of Early Cosmic Evolution, eds. Hill, V.; François, P.; Primas, F., IAUS 228, p. 267
Prantzos, N. 2012, A&A, 542, AA67
Rafelski, M., Wolfe, A. M., Prochaska, J. X., Neeleman, M., & Mendez, A. J. 2012, ApJ, 755, 89
Roederer, I. U., & Kirby, E. N. 2014, MNRAS, 440, 2665
Sandage, A. 2010, ApJ, 722, 79
Sbordone, L., et al. 2010, A&A, 522, A26
Sbordone, L., et al. 2015, A&A, submitted
Schneider, R., Omukai, K., Inoue, A. K., & Ferrara, A. 2006, MNRAS, 369, 1437
Schneider, R., Omukai, K., Bianchi, S., & Valiante, R. 2012a, MNRAS, 419, 1566
Schneider, R., Omukai, K., Limongi, M., et al. 2012b, MNRAS, 423, L60
Schleicher, D. R. G., Banerjee, R., & Klessen, R. S. 2008, Phys. Rev. D, 78, 083005
Schleicher, D. R. G., Banerjee, R., Sur, S., et al. 2010, A&A, 522, AA115
Schober, J., Schleicher, D., Federrath, C., et al. 2012, ApJ, 754, 99
Seifried, D., Banerjee, R., Pudritz, R. E., & Klessen, R. S. 2012, MNRAS, 423, L40
Seifried, D., Banerjee, R., Pudritz, R. E., & Klessen, R. S. 2013, MNRAS, 432, 3320
Sesar, B. 2012, AJ, 144, 114
Shetrone, M. D., Côté, P., & Sargent, W. L. W. 2001, ApJ, 548, 592
Simon, J. D., Jacobson, H. R., Frebel, A., et al. 2015, ApJ, 802, 93
Sivarani, T., Beers, T. C., Bonifacio, P., et al. 2006, A&A, 459, 125
Skúladóttir, Á., Tolstoy, E., Salvadori, S., et al. 2015, A&A, 574, AA129
Smith, R. J., Glover, S. C. O., Clark, P. C., Greif, T., & Klessen, R. S. 2011, MNRAS, 414, 3633
Smith, R. J., Iocco, F., Glover, S. C. O., et al. 2012, ApJ, 761, 154
Spite, M., & Spite, F. 1982, Nature, 297, 483
Spite, M., Cayrel, R., Plez, B., et al. 2005, A&A, 430, 655
Spite, M., Cayrel, R., Hill, V., et al. 2006, A&A, 455, 291
Spite, M., Andrievsky, S. M., Spite, F., et al. 2012a, A&A, 541, A143
Spite, M., Spite, F., & Bonifacio, P. 2012b, Memorie della Società Astronomica Italiana Supplementi, 22, 9
Spite, M., Caffau, E., Bonifacio, P., et al. 2013, A&A, 552, A107
Spite, M., Spite, F., Bonifacio, P., et al. 2014, A&A, 571, AA40
Spolyar, D., Bodenheimer, P., Freese, K., & Gondolo, P. 2009, ApJ, 705, 1031
Stacy, A., & Bromm, V. 2013, MNRAS, 433, 1094
Stacy, A., & Bromm, V. 2014, ApJ, 785, 73
Stacy, A., Greif, T. H., & Bromm, V. 2010, MNRAS, 403, 45
Stacy, A., Bromm, V., & Loeb, A. 2011a, MNRAS, 413, 543
Stacy, A., Bromm, V., & Loeb, A. 2011b, ApJ, 730, LL1
Stacy, A., Greif, T. H., Klessen, R. S., Bromm, V., & Loeb, A. 2013, MNRAS, 431, 1470
Stacy, A., & Bromm, V. 2014, ApJ, 785, 73
Starkenburg, E., Hill, V., Tolstoy, E., et al. 2013, A&A, 549, AA88
Starkenburg, E., Shetrone, M. D., McConnachie, A. W., & Venn, K. A. 2014, MNRAS, 441, 1217
Sur, S., Schleicher, D. R. G., Banerjee, R., Federrath, C., & Klessen, R. S. 2010, ApJ, 721, L134
Tafelmeyer, M., Jablonka, P., Hill, V., et al. 2010, A&A, 524, AA58
Thévenin, F., & Idiart, T. P. 1999, ApJ, 521, 753
Thompson, I. B., Ivans, I. I., Bisterzo, S., et al. 2008, ApJ, 677, 556
Tseliakhovich, D., & Hirata, C. 2010, Phys. Rev. D, 82, 083520
Tseliakhovich, D., Barkana, R., & Hirata, C. M. 2011, MNRAS, 418, 906
Umeda, H., & Nomoto, K. 2003, Nature, 422, 871
Ural, U., Cescutti, G., Koch, A., et al. 2015, MNRAS, 449, 761
Yanny, B., Rockosi, C., Newberg, H. J., et al. 2009, AJ, 137, 4377
Yong, D., Norris, J. E., Bessell, M. S., et al. 2013, ApJ, 762, 26
York, D. G., et al. 2000, AJ, 120, 1579
Zafar, T., Centurión, M., Péroux, C., et al. 2014, MNRAS, 444, 744
Zaggia, S., Bonifacio, P., Bellazzini, M., et al. 2004, Memorie della Societá Astronomica Italiana Supplementi, 5, 291

Table 4. Line-by-line abundances of SDSS J0212+0137, SDSS J1137+2553, and SDSS J1245-0738

				SDSS J0212+0137		SDSS J1137+2553		SDSS J1245-0738	
Ion	λ^a	χ^b	log gf^c	EW^d	A(X)^e	EW^d	A(X)^e	EW^d	A(X)^e
	nm	eV		pm					
Li I	670.7761	0.00	−0.009	synth	2.08	synth	2.30		
Li I	670.7912	0.00	−0.299	synth	2.08	synth	2.30		
O I	777.1941	9.15	0.369	synth	6.70	synth	7.18	synth	7.30
O I	777.4161	9.15	0.223	synth	6.70	synth	7.18	synth	7.30
O I	777.5388	9.15	0.001	synth	6.70	synth	7.18	synth	7.30
Na I	588.9951	0.00	0.117			synth	6.10	synth	4.00
Na I	589.5924	0.00	−0.184			synth	6.30	synth	4.50
Mg I	382.9355	2.71	−0.231	synth	4.45	synth	6.17	synth	5.30
Mg I	383.2304	2.71	0.146	synth	4.55	synth	6.17		
Mg I	383.8290	2.72	0.415	synth	4.60	synth	6.17	synth	4.80
Al I	394.4006	0.00	−0.623	synth	2.34		3.30		
Al I	396.1520	0.01	−0.323	synth	2.28	7.14	3.30	8.47	3.10
Si I	390.5523	1.91	−1.041	synth	4.15	synth	5.10	synth	4.30
Ca I	422.6728	0.00	0.244	7.86	3.35	11.59	4.24	synth	3.05
Ca I	445.4779	1.90	0.258	1.06	3.36	4.17	4.17	synth	4.00
Ca II	393.3663	0.00	0.105	synth	3.50	synth	4.15	synth	3.97
Ca II	396.8469	0.00	−0.200	synth	3.55	synth	4.15	synth	4.00
Ca II	849.8023	1.69	−1.416	synth	3.80	synth	4.60	synth	4.20
Ca II	854.2091	1.70	−0.463	synth	4.00				
Ca II	866.2170	1.69	−0.723	synth	4.00				
Sc II	424.6822	0.31	0.242	1.48	0.00	7.19	1.03	6.04	0.16
Ti II	375.9291	0.61	0.280			10.42	2.72	12.92	1.90
Ti II	376.1320	0.57	0.180	7.02	2.13	9.74	2.60	14.24	2.24
Ti II	391.3461	1.12	−0.420	2.34	2.08	5.29	2.43	5.71	1.96
Ti II	441.7714	1.16	−1.190	.56	2.11	2.23	2.54		
Ti II	444.3794	1.08	−0.720	.82	1.74	3.45	2.27	5.09	2.09
Ti II	444.4555	1.12	−2.240			0.72	2.97		
Ti II	445.0482	1.08	−1.520						
Ti II	446.8507	1.13	−0.600	1.63	2.01	4.41	2.38		
Ti II	450.1270	1.12	−0.770	1.30	2.05	3.32	2.32		
Ti II	453.3960	1.24	−0.530	1.23	1.89	4.70	2.46	8.10	2.42
Ti II	456.3757	1.22	−0.690	1.13	1.99	3.20	2.31	6.46	2.36
Ti II	457.1968	1.57	−0.320	1.04	1.90	3.64	2.35	2.45	1.72
Cr I	425.4336	0.00	−0.114	1.32	2.09	5.24	3.03	2.41	2.17
Fe I	375.8233	0.96	−0.027			9.88	5.00		
Fe I	376.3789	0.99	−0.238	4.93	3.85	9.39	5.10	11.51	4.37
Fe I	376.5539	3.24	0.482			3.55	4.78		
Fe I	376.7192	1.01	−0.389	4.05	3.81	7.02	4.52	7.03	3.84
Fe I	378.7880	1.01	−0.859	2.78	3.97	6.37	4.79	12.08	5.11
Fe I	380.5342	3.30	0.312						
Fe I	381.5840	1.49	0.237	5.27	3.90	8.90	4.88	7.04	3.66
Fe I	382.0425	0.86	0.119	7.42	4.07	10.31	4.84	7.64	3.27
Fe I	382.4444	0.00	−1.362	4.84	4.04	8.39	5.02	6.94	3.84
Fe I	382.5881	0.92	−0.037	5.98	3.85				
Fe I	382.7822	1.56	0.062	4.27	3.89	7.57	4.71	13.13	4.90
Fe I	384.0437	0.99	−0.506	3.59	3.79	8.40	5.02		
Fe I	384.9966	1.01	−0.871	2.39	3.88	7.75	5.20	12.95	5.27
Fe I	385.0818	0.99	−1.734	0.89	4.19	4.04	5.08		
Fe I	385.6371	0.05	−1.286	5.04	4.06	8.75	5.11	9.38	4.15
Fe I	385.9911	0.00	−0.710	7.67	4.22	9.46	4.73	9.44	3.53
Fe I	386.5523	1.01	−0.982	2.31	3.97	5.92	4.78	8.03	4.55
Fe I	387.8018	0.96	−0.914	2.65	3.94	6.21	4.73		
Fe I	389.9707	0.09	−1.531	4.07	4.09	7.06	4.81		
Fe I	392.0258	0.12	−1.746	2.26	3.90	6.24	4.81	3.18	3.80
Fe I	392.2912	0.05	−1.651	2.93	3.91	8.08	5.22	9.55	4.53
Fe I	400.5242	1.56	−0.610	2.41	4.10	4.65	4.58	2.83	3.94
Fe I	404.5812	1.49	0.280	5.70	3.93	8.87	4.78	7.61	3.66
Fe I	406.3594	1.56	0.062	4.48	3.91	8.04	4.80	9.94	4.27

Table 4. continued.

Ion	λ^a nm	χ^b eV	log gf^c	SDSS J0212+0137 EW^d pm	SDSS J0212+0137 A(X)^e	SDSS J1137+2553 EW^d	SDSS J1137+2553 A(X)^e	SDSS J1245-0738 EW^d	SDSS J1245-0738 A(X)^e
Fe I	407.1738	1.61	−0.022	3.39	3.79	7.75	4.84	8.22	4.15
Fe I	413.2058	1.61	−0.675	1.09	3.76	5.55	4.88	4.03	4.24
Fe I	414.3868	1.56	−0.511	1.93	3.86	5.23	4.60	8.86	4.67
Fe I	415.6799	2.83	−0.809			1.20	5.03		
Fe I	418.7039	2.45	−0.548	0.51	4.02	2.22	4.76		
Fe I	418.7795	2.42	−0.554			2.68	4.86	2.79	4.66
Fe I	419.1430	2.47	−0.666			1.32	4.61	2.43	4.74
Fe I	419.9095	3.05	0.155	0.51	3.86	3.16	4.82	2.21	4.40
Fe I	420.2029	1.49	−0.708	1.66	3.90	6.07	4.93	5.51	4.36
Fe I	422.7427	3.33	0.266			3.05	4.94		
Fe I	425.0119	2.47	−0.405			2.60	4.73		
Fe I	426.0474	2.40	0.109	1.27	3.76	5.92	4.88	2.52	3.92
Fe I	438.3545	1.49	0.200	5.55	3.93	8.97	4.82	8.39	3.81
Fe I	440.4750	1.56	−0.142	3.52	3.86	7.08	4.67	9.01	4.30
Fe I	444.3194	2.86	−1.043			0.73	5.03		
Fe I	446.6551	2.83	−0.600			1.96	5.07		
Fe I	452.8614	2.18	−0.822	0.83	4.26	2.54	4.85	2.86	4.69
Fe I	489.1492	2.85	−0.112			3.52	4.95		
Fe I	490.3310	2.88	−0.926			0.97	5.05		
Fe I	491.8994	2.87	−0.342	0.61	4.23	1.30	4.59	1.34	4.45
Fe I	492.0502	2.83	0.068	0.63	3.81	2.99	4.63	4.63	4.68
Fe II	423.3172	2.58	−1.947			2.65	4.60	3.08	4.33
Fe II	441.6830	2.78	−2.602			1.24	4.99		
Fe II	449.1405	2.86	−2.756			0.25	4.46		
Fe II	452.0224	2.81	−2.617			0.45	4.54		
Fe II	454.1524	2.86	−2.973			0.46	4.95		
Fe II	455.5893	2.83	−2.421			1.89	5.07	1.41	4.61
Fe II	492.3927	2.89	−1.504	0.65	3.93	4.98	4.90	4.15	4.31
Co I	384.5461	0.92	0.010					3.00	2.64
Co I	399.5302	0.92	−0.220			2.33	2.97		
Co I	412.1311	0.92	−0.320	0.78	2.49			2.83	2.91
Ni I	380.7138	0.42	−1.205	0.90	2.82	2.11	3.25		
Ni I	385.8292	0.42	−0.936	1.27	2.72	4.10	3.44	5.48	3.29
Sr II	407.7709	0.00	0.167	2.58	−0.87	12.14	1.40	11.93	−0.17
Sr II	421.5519	0.00	−0.145	1.36	−0.96	11.64	1.60	7.26	−0.60
Ba II	413.0645	2.72	*hfs*			synth	1.90		
Ba II	455.4029	0.00	*hfs*	synth	−1.40	synth	2.55	synth	0.35
Ba II	493.4829	1.25	*hfs*			synth	2.55	synth	0.10
Ba II	585.3668	0.60	*hfs*			synth	1.88		
Ba II	614.1713	0.70	*hfs*			synth	2.45		
Ba II	649.6897	0.60	*hfs*			synth	2.50		

[a] Wavelength
[b] Lower energy of the transition
[c] Logarithm of the product of the oscillator strength of the transition and the statistical weight of the lower level
[d] Equivalent width of the line
[e] Abundance of the element A(X) = log (X/H) + 12

Appendix A: Ratios of various elements to calcium

For the reader's convenience we present in the following table the data that were used to plot Fig. 7. All the published ratios have been scaled to bring them to our adopted solar abundance scale. As solar reference for carbon, nitrogen, oxygen, and iron we took Caffau et al. (2011a), and for the other elements Lodders et al. (2009).

Table A.1. [X/Ca] ratios for the four low-carbon band stars studied in the present paper and for the carbon-normal most metal-poor star SDSS J1029+1729.

	Z	(1)	(2)	(3)	(4)	(5)
[C/Ca]	6	+1.43	+3.23	+3.38	+3.32	-
[N/Ca]	7	+1.85	-	-	-	-
[O/Ca]	8	+0.75	-	-	-	-
[Na/Ca]	11	-	-	-	-	-
[Mg/Ca]	12	-0.35	-	-	-	-0.11
[Al/Ca]	13	-1.38	-	-	-	-
[Si/Ca]	14	-0.39	-	-	-	+0.33
[Sc/Ca]	21	-0.29	-	-	-	-
[Ti/Ca]	22	-0.10	-	-	-	-0.15
[Cr/Ca]	24	-0.74	-	-	-	-
[Mn/Ca]	25	-	-	-	-	-
[Fe/Ca]	26	-0.78	-	-	-0.24	-0.13
[Co/Ca]	27	+0.38	-	-	-	-
[Ni/Ca]	28	-0.65	-	-	-	+0.05
[Sr/Ca]	38	-1.02	-	-	-	-
[Ba/Ca]	56	-0.62	-	-	-	-

(1) SDSS J0212+0137 This paper
(2) SDSS J0929+0238 This paper
(3) SDSS J1035+0641 This paper
(4) SDSS J1742+2531 This paper
(5) SDSS J1029+1729 Caffau et al. (2012)

Table A.2. The [X/Ca] ratios for all the known CEMP stars with [Fe/H] less than about –4.0. All the published abundances have been scaled to our adopted solar values.

	Z	(1)	(2)	(3)	(4)	(5)	(6)	(7)	(8)	(9)	Mean	σ	Min.	Max.
[C/Ca][a]	6	+3.20	+0.82	+3.06	+4.72	+2.53	+0.94	+2.28	+3.39	+0.82	+2.44	+1.04	+0.82	+3.39
[N/Ca][a]	7	+2.25	+0.86	-	-	+1.57	-	+3.16	+3.92	+2.26	+2.35	+1.22	+0.86	+3.92
[O/Ca]	8	+1.79	-	-	-	+1.57	-	-	+3.07	+1.68	+2.18	+0.77	+1.68	+3.07
[Na/Ca]	11	+0.45	-0.41	-	-	+0.03	-0.89	+0.12	+1.68	+1.10	+0.33	+0.87	-0.89	+1.68
[Mg/Ca]	12	-0.24	+0.20	+0.30	+2.95	-0.11	-0.36	+0.47	+0.99	+1.23	+0.26	+0.53	-0.36	+1.23
[Al/Ca]	13	-	-	-	-	-	-1.31	-0.42	+0.42	-0.53	-0.56	+0.73	-1.31	+0.42
[Si/Ca]	14	-	-0.07	+0.01	-	-	-	-	-	+0.13	+0.10	+0.17	-0.07	+0.33
[Sc/Ca]	21	-	-0.16	-	-	-	-0.34	-0.18	-	-0.20	-0.16	+0.17	-0.34	+0.07
[Ti/Ca]	22	-0.63	+0.05	-0.12	-	-	-0.25	+0.39	-0.00	+0.11	-0.10	+0.26	-0.63	+0.18
[Cr/Ca]	24	-	-0.33	-	-	-0.21	-1.30	-0.50	-	-0.75	-0.53	+0.51	-1.30	-0.01
[Mn/Ca]	25	-	-1.24	-	-	-0.64	-	-1.35	-	-1.16	-1.05	+0.41	-1.35	-0.44
[Fe/Ca]	26	-0.57	-0.13	-0.37	-	-0.67	-0.60	-0.03	-0.74	-0.41	-0.39	+0.21	-0.74	-0.13
[Co/Ca]	27	-	+0.21	-	-	-	-0.57	+0.16	-	-0.04	-0.06	+0.36	-0.57	+0.21
[Ni/Ca]	28	-0.74	+0.07	-	-	-	-0.82	-0.14	-0.51	-0.44	-0.34	+0.38	-0.82	+0.07
[Sr/Ca]	38	-	-0.46	-0.08	-	-	-	-1.14	+0.31	-0.04	-0.28	+0.55	-1.14	+0.31
[Ba/Ca]	56	-	-	-	-	-	-	-0.50	-	-0.99	-0.75	+0.35	-0.99	-0.50

(1) HE 0107-5240 Christlieb et al. (2004)
(2) HE 0134-1519 Hansen et al. (2014)
(3) HE 0233-0343 Hansen et al. (2014)
(4) SMSS J0313-6708 Keller et al. (2014)
(5) G 77-61 Plez & Cohen (2005); Plez et al. (2005)
(6) HE 0557-4840 Norris et al. (2007)
(7) HE 1310-0536 Hansen et al. (2014)
(8) HE 1327-2326 Frebel et al. (2008)
(9) CS 22949-037 Depagne et al. (2002); Norris et al. (2002)
[a] For these elements the abundances of CS 22949-037 have not been considered to compute the mean and σ since the star is “mixed”, in the sense of Spite et al. (2005).

Table A.3. Abundances of Fe, Ca, and C for the sample of nine comparison stars.

Star	[Fe/H]	[Ca/H]	A(C)
HE 0107-5240	−5.46	−4.89	6.81
HE 0134-1519	−4.00	−3.87	5.45
HE 0233-0343	−4.70	−4.33	7.23
SMSS J0313-6708	< −7.32	−7.19	6.03
G 77-61	−4.10	−3.43	7.60
HE 0557-4840	−4.75	−4.15	5.29
HE 1310-0536	−4.17	−4.14	6.64
HE 1327-2326	−5.73	−4.99	6.90
CS 22949-037	−4.01	−3.60	5.72